



1 Properties of exopolymeric substances (EPS) produced during cyanobacterial growth: potential role 2 in whiting events

3 Marliisa Martinho de Brito^{1*}, Irina Bundeleva¹, Frédéric Marin¹, Emmanuelle Vennin¹, Annick Wilmotte², Laurent Plasseraud³ and Pieter T. Visscher^{1,4}.

4 ¹Biogeosciences Laboratory, Department of Life, Earth and Environmental Sciences, University of Bourgogne Franche-Comté, 21000 Dijon, France

5 ²InBios Research Unit, Department of Life Sciences, Faculty of Sciences, University of Liège, 4000 Liège, Belgium

6 ³ICMUB Institute of Molecular Chemistry (CNRS UMR CNRS 6302), University of Burgundy-Franche-Comté, 21000 Dijon, France

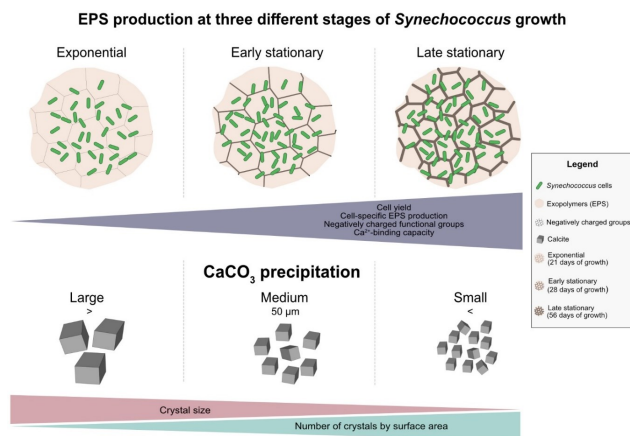
7 ⁴Department of Marine Sciences, The University of Connecticut, Groton, CT 06340, USA

8 Correspondence to: Marliisa Martinho de Brito (marliisa_de-brito@etu.u-bourgogne.fr)

9 Abstract

10
11
12
13
14
15
16 Extracellular polymeric substances (EPS) are an important organic carbon reservoir in many pelagic and benthic environments. The production of EPS is intimately
17 associated with the growth of phyto- and picoplankton. EPS plays a critical role in carbonate precipitation through the binding of cations and by acting as a nucleation
18 site for minerals. Large-scale episodes of fine-grained calcium carbonate precipitation in the water column (whiting events) have been linked to cyanobacterial blooms,
19 including of *Synechococcus* spp.. The mechanisms that trigger these precipitation events are still debated. We pose that the cyanobacterial EPS, produced during
20 exponential and stationary growth phases plays a critical role in the formation of whittings. The aim of this study was to investigate the production of EPS during a
21 two-month cyanobacterial growth, mimicking a bloom. We further evaluated the potential role of EPS in carbonate precipitation. The production and properties of
22 EPS produced at different *Synechococcus* spp., growth stages were investigated and carbonate mineral formation within these EPS matrices was determined in forced
23 precipitation experiments. EPS produced during the early and late stationary phase contained a larger amount of negatively charged groups than present in EPS
24 produced during the exponential phase. Consequently, a higher Ca²⁺ binding affinity of the stationary phase-EPS led to the formation of a larger amount of smaller
25 carbonate minerals (<50 μm) compared to crystals formed in exponential phase-EPS, which were less and larger (> 50 μm). These findings were used to establish a
26 conceptual model for picoplankton bloom-mediated CaCO₃ precipitation that can explain the role of EPS in whittings (see graphical abstract).

27 Graphical abstract



46 1. Introduction

47 1.1 Significance of this study

48 Massive carbonate precipitation episodes in the water column, also referred to as 'whittings events' are a well-known phenomenon of modern freshwater (Schultze-
49 Lam et al., 1997; Hodell et al., 1998; Stanton et al., 2021) and marine environments (Shinn et al., 1989; Robbins and Blackwelder, 1992; Larson and Mylroie, 2014).
50 Whittings are caused by large-scale precipitation of micron-sized calcium carbonate particles (visible from space) and represent a major sink in the carbon cycle. The
51 particles associated with whittings can make up a major sedimentary constituent of the modern-day and ancient carbonate rock records (Pomar and Hallock, 2008).
52 Whiting events can be triggered by a combination of biological and physicochemical processes. Among the biological mechanisms that have been studied in this
53 context, picocyanobacterial proliferations also known as blooms (Huisman et al., 2018) have often been invoked in the initiation of whittings (Thompson and Ferris,
54 1990; Hodell et al., 1998; Thompson, 2000; Obst et al., 2009). The process of photosynthesis results in an increase of pH levels and alkalinity during cyanobacterial
55 blooms, ultimately causing the saturation state of calcium carbonate to rise, thereby leading to its potential precipitation. The role of *Synechococcus* spp. bloom-
56 forming cyanobacteria in CaCO₃ precipitation has been demonstrated in laboratory experiments (Yates and Robbins, 1998; Dittrich et al., 2003; Obst et al., 2009;
57 Bundeleva et al., 2014; Martinho de Brito et al., 2022) and observed in field investigations (Wells and Iling, 1964; Thompson et al., 1990; Dittrich and Obst., 2004).
58 Change in temperature, salinity, CO₂ pressure as well as turbulence are some of the physicochemical factors can lead to the formation of supersaturated solutions and
59 subsequent precipitation of CaCO₃ thus initiating the whiting. Even though several possible biogenic and abiotic mechanisms have been identified, the formation of
60 whittings is still poorly understood.



61 1.2 Overview of phytoplankton blooms

62 Phytoplankton blooms, including those of picoplankton, are dense accumulations of cells resulting in a visible discoloration of the surface water layers (Reynolds and
63 Walsby, 1975; Huisman et al., 2018). Their occurrence has been recorded worldwide in marine and freshwater bodies (Paerl et al., 2001; Paerl and Huisman, 2008;
64 Ploug, 2008). Light intensity, water temperature, nutrient availability, weather conditions and hydrodynamics are key factors that determine the onset and persistence
65 of a bloom. Blooms are typically seasonal, frequently observed during late spring or summer, and can be dominated by picoplankton (Huisman et al., 2018). Some
66 phytoplankton organisms, notably cyanobacteria, may produce toxins and form large-scale harmful algal blooms (Paerl et al., 2001). The intensity and frequency of
67 cyanobacterial blooms have been increasing due to anthropogenic eutrophication (Heisler et al., 2008; O'Neil et al., 2012), a trend expected to exacerbate due to
68 climate change (Lüring et al., 2018). Cyanobacteria comprise a diverse group of photoautotrophic organisms that play a pivotal role in global primary production and
69 are key players in the biogeochemical cycles of carbon, nitrogen and oxygen (Callieri and Stockner, 2000; Whitton and Potts, 2012; Raven et al., 2017). The unicellular
70 cyanobacterium *Synechococcus* is one of the most abundant photosynthetic microorganisms on Earth (Whitton and Potts, 2012), which contribute substantially to the
71 picoplankton community in marine (Murphy and Haugen, 1985; Coello-Camba and Agustí, 2021) and freshwater environments (Weisse, 1993) that can form dense
72 blooms (Schultze-Lam et al., 1992; Philips et al., 1999; Dittrich and Obst, 2004b).

73 1.3 Phytoplankton blooms and CaCO₃ precipitation

74 During the occurrence of dense phytoplankton blooms, high rates of photosynthetic activity lead to a rapid depletion of CO₂ in the surface waters, increasing alkalinity.
75 Depending on the buffering capacity of the water, this could result in pH values ≥ 9 to as high as 11 (Ibelings and Maberly, 1998; Zepernick et al., 2021). Consequently,
76 the inorganic carbonate equilibrium shifts towards carbonate (CO₃²⁻). Some cyanobacteria possess a carbon concentrating mechanism (CCM) that converts HCO₃⁻ to
77 CO₂ through the action of carbonic anhydrase enzymes (Price et al., 1998; Badger et al., 2002) and produce hydroxide ions (Kupriyanova and Pronina, 2011). The
78 activity of extracellular carbonic anhydrase (eCA) may contribute to the create an alkaline microenvironment in the extracellular polymeric substances (EPS)
79 surrounding the cyanobacterial cells (Price et al., 2002; Dupraz et al., 2009). When OH⁻ ions are released during photosynthesis it causes the pH to rise, which favors
80 carbonate mineral precipitation, assuming there is enough calcium ions available (Kamennaya et al., 2012). Consequently, during blooms, carbonate minerals can
81 form on EPS or precipitated in the microenvironment surrounding cyanobacterial cells.

82 1.4 The role of EPS

83 Cyanobacteria are known producers of EPS (De Philippis et al., 2001; Pereira et al., 2009; Dittrich and Sibling, 2010), especially during blooms (Pannard et al., 2016;
84 Liu et al., 2018). EPS serve as a boundary between cells and their immediate environment (Whitton and Potts, 2012) and may act as a template for CaCO₃ nucleation
85 (Dupraz and Visscher, 2005; Dupraz et al., 2009; Kamennaya et al., 2012). EPS are high molecular weight organic molecules composed of polysaccharides, proteins,
86 nucleic acids and lipids (Pereira et al., 2009; Marvasi et al., 2010; Decho and Gutierrez, 2017). This complex mixture of molecules may contain specific monomers
87 components, such as uronic or sialic acids (monosaccharides), aspartic or glutamic acids (amino acids) or functions (sulfate, phosphate), which carry negative charges
88 in physiological conditions and can therefore bind cations, such as Ca²⁺, and promote the nucleation of CaCO₃ crystals (Trichet and Defarge, 1995; Braissant et al.,
89 2003; Dupraz et al., 2009; Dittrich and Sibling, 2010; Walker et al., 2019). Conversely, polyanionic EPS in solution can inhibit crystal growth by poisoning the faces
90 of growing nuclei by an adsorption mechanism, according to a classical and accepted view prevailing for other macromolecules of similar charge properties: synthetic
91 peptides (Wheeler et al., 1991), skeletal proteins (Wheeler et al., 1981; Addadi and Weiner, 1985), coccolith-associated polysaccharides (Borman et al., 1982) or
92 natural organic matter dissolved in seawater (Mitterer and Cunningham, 1985). The production and composition of EPS differ among different species of
93 microorganisms and their type of metabolism and depend on environment in which they live and stresses (e.g., nutrient availability, pH, temperature, light, salinity)
94 and the stage of their growth (Pereira et al., 2009; Pannard et al., 2016; Martinho de Brito et al., 2022). The deprotonation of functional groups at elevated pH enhances
95 the binding capacity of cations such as Ca²⁺ and controls crystal nucleation and growth by reducing the interfacial energy barrier between the crystal and the EPS
96 substrate (Dupraz et al., 2009; Dittrich and Sibling, 2010). EPS play a two-fold role in carbonate formation by initially inhibiting (through Ca²⁺ binding) and subsequently
97 promoting carbonate precipitation by releasing calcium ions during EPS alteration and degradation (Dupraz and Visscher, 2005; Dupraz et al., 2009). Furthermore,
98 through specific functional group composition and structural architecture, EPS may also exert control over the mineralogy, morphology and/or abundance of the
99 minerals that are formed (Trichet and Defarge, 1995; Dupraz et al., 2009).

100 1.5 The goal of this study

101 We have previously reported that the pH of *Synechococcus* cultures increased when grown in a non-buffered medium (Martinho de Brito et al., 2022). In these growth
102 conditions, the production of EPS was enhanced compared to growth in a buffered medium. Furthermore, the EPS from cells grown in non-buffered conditions
103 contained more negatively-charged functional groups that impacted the properties of the carbonate minerals that precipitated (Martinho de Brito et al., 2022). The
104 current study further investigates the properties of EPS produced during different growth phases of *Synechococcus* spp. Over an extended incubation time (mimicking
105 a prolonged natural bloom). We aim to better understand the role of cyanobacterial blooms in carbonate precipitation through EPS production and develop a conceptual
106 model of picoplankton-mediated organomineralization to explain the biological origin of whitening events.

107 2. Materials and Methods

108 2.1 *Synechococcus* PCC7942 strain and culture growth conditions

109 *Synechococcus* PCC7942 was obtained from the Centre de Ressources Biologiques de l'Institut Pasteur (Paris). Cultures were grown in a one-third-strength, non-
110 buffered liquid BG-11 medium (Allen, 1968; Rippka et al., 1979). The medium consists of (per liter): 1.5 g of NaNO₃; 0.04 g of K₂HPO₄·2H₂O; 0.075 g of MgSO₄·7H₂O;
111 0.036 g of CaCl₂·2H₂O; 6 mg of citric acid combined with 6 mg of ferric citrate; 0.001 g of Na₂EDTA·2H₂O and 0.02 g of Na₂CO₃. Trace metal solutions contained
112 (per liter) 2.86 mg of H₃BO₃; 1.81 mg of MnCl₂·4H₂O; 0.222 mg of ZnSO₄·7H₂O; 0.39 mg of Na₂MoO₄·2H₂O; 0.079 mg of CuSO₄·5H₂O and 0.0494 mg of
113 Co(NO₃)₂·6H₂O. Cultures were incubated at room temperature (21°C±2), in a light/dark cycle of 12h/12h under 36.8 μE m⁻² s⁻¹ of photon irradiance while shaken at
114 200 rpm in a Cimarec i Multipoint Stirrer, 6 Position, 2000 rpm, 3L per Multipoint, 100-240 VAC rotary shaker.



115 2.2 Experimental design of *Synechococcus*-bloom formation

116 Two independent growth experiments were performed in 1L glass serum bottles containing 800 mL of $\frac{1}{3}$ BG-11 medium adjusted to pH 7.5, sealed with silicone caps
117 to allow gas exchange. Cells used for the inoculum (pH = 9.2) were pre-cultured in a full-strength BG-11. Immediately after inoculation (30 mL/bottle), the pH
118 increased to approximately 8.2.

119 2.2.1 Experiment I

120 In the first growth experiment, six bottles were inoculated with *Synechococcus* PCC7942. Cell growth and EPS production were examined. Optical density (OD_{750nm}),
121 pH and cell counts were monitored weekly (2-3 times by week). EPS was extracted on days 14, 28 and 56 of cultivation (two bottles were harvested at each sampling
122 time).

123 2.2.2 Experiment II

124 The second growth experiment was performed in quadruplicate. Chlorophyll *a* (Chl_a), extracellular carbonic anhydrase activity (eCA), nutrients (NO_3^- and PO_4^{3-}) and
125 calcium concentration were analysed at 0, 14, 28 and 56 days of cultivation. pH values, OD and cell counts were also assessed at longer intervals (once per week) than
126 in Experiment I.

127 2.3 Growth assessment

128 2.3.1 Optical density, cell counts and pH values

129 The pH value was measured with a CRISON GLP 21 pH meter (Crison Instruments SA, Alella, Spain). Cell growth was monitored through cell counts and OD_{750}
130 measurements. Cell counts were performed using a counting chamber (Neubauer, Mariangela, Germany) by randomly selecting five fields of view and counting
131 approximately 100-200 cells. The OD at 750 nm of a 1-ml sample of the culture was measured in a Bio-Rad SmartSpec Plus Spectrophotometer (Bio-Rad, Hercules,
132 CA, USA).

133 2.3.2 Chlorophyll-a extraction

134 Chl_a was extracted from 2 ml culture aliquots using a methanol extraction method (Stal et al., 1984). Following the extraction in the dark at 4 °C, samples were
135 centrifuged. The Chl_a absorbance was measured in the supernatant at 665 nm using a Bio-Rad SmartSpec Plus Spectrophotometer (Bio-Rad, Hercules, CA, USA).

136 2.3.3 Extracellular carbonic anhydrase activity

137 The extracellular carbonic anhydrase (eCA) activity was measured using a BioVision Carbonic Anhydrase Activity Assay Kit Kit (BioVision, Ref. K472-100, Abcam,
138 Waltham, MA, USA) according to the manufacturer's specifications. Aliquots of ~ 5 ml were analysed immediately after the collection. To avoid cell lysis and
139 intracellular CA contamination, samples were not centrifuged. The cells were separated from the supernatant by using a 1 mL syringe and a 0.20 µm NALGENE®
140 syringe filter. The absorbance was measured in a Bio-Rad Model 680 Microplate Reader at 405 nm.

141 2.3.4 Nitrogen, phosphorus and calcium measurements

142 Phosphate, nitrate, nitrite and calcium concentrations were determined in the growth medium at 0, 14, 28 and 56 days of cultivation. Cells were removed by
143 centrifugation and filtration through a 0.20 µm Millipore filter under a mild vacuum. The samples were stored at 4°C in the dark until measured by ion chromatography.
144 Analyses were realized within the PEA² technical platform of the Chrono-Environment Laboratory UMR6249 (Université de Franche-Comté, Besançon, France) and
145 the Ca^{2+} concentration was determined by ICP-AES (dual axial and radial view iCAP Pro XP model with fast loop, Thermofisher Scientific, Courtaboeuf, France)
146 available at the University of Franche-Comté, Besançon, France.

147 2.4 EPS extraction and purification

148 EPS were extracted from the *Synechococcus* cultures as previously described by Martinho de Brito et al. (2022). EPS were harvested after 14, 28 and 56 days of
149 cultivation. Cyanobacterial cells were inspected by microscopy to ensure that no cell lysis had occurred during the extraction process. The pure EPS fractions were
150 obtained by ultrafiltration (>10 kDa = retentate) for volume reduction and the weight of the material was determined following by dialysis (using a 1 kDa Membrane)
151 lyophilization on a high-precision analytical balance (Quintix 35-1S, Sartorius, Gottingen, Germany).

152 2.5 EPS characterization

153 2.5.1 Fourier Transform-Infrared Spectroscopy

154 FT-IR spectra were obtained from freeze-dried EPS on an FT-IR Bruker Alpha spectrometer (Bruker Optics SARL, Marne la Vallée, France) fitted with an Attenuated
155 Total Reflectance (ATR) ALPHA-P device equipped with a mono-reflection diamond crystal. A total of 24 scans were performed on each sample at a spectral
156 resolution of 4 cm^{-1} in the 4000–375 cm^{-1} wavenumber range. The qualitative assignment of absorption bands was performed by comparison with spectra available in
157 the literature (Coates, 2000).

158 2.5.2 Protein, sugar and glycosaminoglycan [quantification]

159 The total protein content of EPS was determined using the Bicinchoninic acid assay (Pierce® BCA Protein Assay Kit) and bovine serum albumin as the standard. The
160 total sugar content was determined by a modified phenol-sulfuric acid method (Dubois et al., 1956) and xanthan and dextran were used as standards (Sigma-Aldrich,
161 St. Louis, MO, USA). The total glycosaminoglycan (GAGs) content was quantified using the Blyscan Assay according to the manufacturer's protocol (Blyscan Kit
162 B1000, Biocolor Ltd., Antrim, UK) with chondroitin sulphate as the standard. All assays were carried out in duplicate.



163 **2.5.3 Visualization of polyanionic macromolecules on Alcian Blue stained gels**

164 Sodium Dodecyl Sulfate-Polyacrylamide Gel Electrophoresis (SDS-PAGE) followed by Alcian Blue staining (Wall and Gyi, 1988) were used to separate and to stain
165 negatively charged macromolecules (10- > 170 kDa), respectively. Alcian Blue is a dye that specifically binds to glycoconjugates with an acidic character (e.g.,
166 containing carboxylated or sulfated functional groups). Samples were analysed on one-dimensional precast gradient protein gels (TGX Gel 4-15%, 90 mm x 70 mm)
167 on a Mini-Protean 3 cell (Bio-Rad, Hercules, CA, USA), according to the method previously described by Martinho de Brito et al. (Martinho de Brito et al., 2022).
168 Prior to migration, samples were heat-denatured in standard 2xLaemmli sample buffer (5 min., 99°C, ref. 1610737, Bio-Rad). A pre-stained protein ladder (Euromedex,
169 #06P-0111; MW: 10 kDa to > 170 kDa) was used as a reference.

170 **2.5.4 Inhibitory effect of EPS using pH-drift assay**

171 The capacity of negatively charged functional groups in EPS to inhibit the *in vitro* precipitation of calcium carbonate was tested with the pH-drift assay (Wheeler et
172 al., 1981; Marin et al., 2000; Kawaguchi and Decho, 2002). This assay was performed as previously described by Martinho de Brito et al. (2022). Briefly, the pH was
173 recorded by a pH meter (Laboratory Research Grade Benchtop pH/mV Meter with 0.001 pH Resolution-HI5221) connected to a PC via a USB cable. Data were
174 recorded by the HANNA HI92000 software. The pH was measured every 2 s for 15 min. The shape of the curve (after reaching its maximum, about one minute after
175 T0) reflects directly the inhibitory capacity of the tested EPS: a fast decrease in pH (decreasing exponential) indicates ongoing precipitation, i.e. the absence of
176 inhibition, while a delayed decrease, resulting in a plateau around pH 8, means an inhibitory effect, proportional to the length of the plateau. Between each experiment,
177 the electrode was refreshed with dilute acid and blank tests (without EPS) were performed.

178 **2.6 Interaction of EPS with the *in vitro* precipitation of CaCO₃**

179 The potential of the EPS matrix to interact with the precipitation of calcium carbonate was tested via the diffusion method in the presence of a closed ammonia-CO₂
180 saturated atmosphere (Albeck et al., 1993). 200 µL of the mixture containing pre-filtered (0.22 µm) CaCl₂ solution (10 mM) and EPS at increasing concentrations (3,
181 18, and 36 µg.mL⁻¹) were incubated in duplicate in 16-well plates (Lab-Tek, Nunc/Thermo Scientific, Rochester, NY, USA). The EPS concentrations were selected
182 to match the EPS yields at the extraction times (14, 28 and 56 days of cultivation). The plastic covers of the well plates were perforated to allow the reaction between
183 CaCl₂ solutions containing EPS and ammonium bicarbonate. The well plates were placed in a desiccator that was incubated at 4°C in the dark for 72 hrs. At the
184 completion of the incubation period, the pH value was measured in each well and the overlying solutions were carefully removed to dryness and CaCO₃ crystals
185 analysed. Blank experiments were performed without any EPS. The experiment was carried out in duplicates.

186 **2.6.1 Morphology and mineralogy of the crystals**

187 The 16-well plates containing crystals were used in two manners: first, the morphology of the CaCO₃ crystals was checked with a tabletop scanning electron microscope
188 (Hitachi TM 1000, Ibaraki, Japan) in back-scattered electron mode. To this end, the glass plate base was unsealed from its plastic well part and directly observed
189 without carbon or gold sputtering. Secondly, the polymorph of the calcium carbonate minerals was determined by FT-IR spectroscopy using an FT-IR Bruker Alpha
190 (Bruker Optics, SARRL, Champs-sur-Marne, France). Mineral phases were determined by comparison of the spectra with the reference spectra available in the RRUFF
191 Project database (<https://rruff.info>, accessed on January 1st, 2022).

192 **2.6.2 Crystal counts and size distribution**

193 CaCO₃ crystals were counted directly in the 16-well plates using an inverted microscope (Nachet, Paris, France) equipped with Mosaic 2.2.1 image analysis software.
194 Images were processed to obtain crystal sizes (average width and length of size classes < 50 µm and > 50 µm) and the total count of crystals in each well. A total of
195 ten fields of view accounting for 15.5 mm² were analysed. The results are reported as the mean ± standard error of the mean.

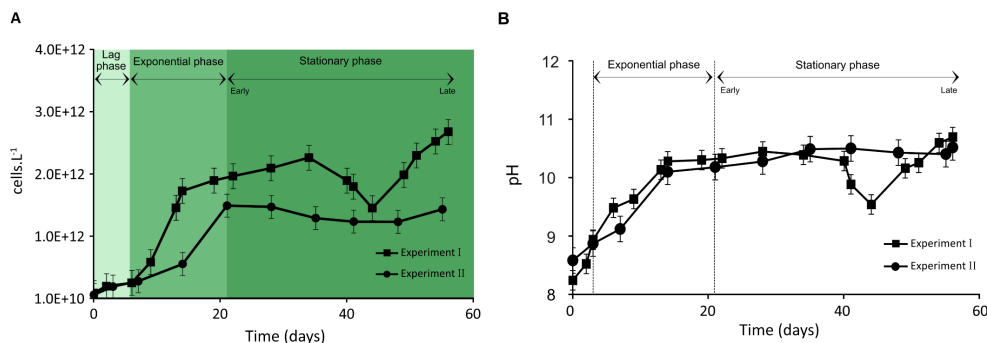
196 **2.7 Statistical analysis**

197 All the data concerning *Synechococcus* growth and EPS production are representative of two independent experiments with two technical replicates (four replicates
198 for EPS extracted at 56 days of culture). The results are reported as the mean ± standard error of the mean. Statistical significance was assessed by performing single-
199 factor ANOVA tests; p-values < 0.05 were statistically different.

200 **3. Results**

201 **3.1 Trends in *Synechococcus* PCC7942 growth experiments and pH evolution**

202 Cell density and pH values increased over the *Synechococcus* cultivation period (Figure 1A and 1B). The growth of *Synechococcus* cells showed a typical pattern
203 including a brief lag phase (~6-7 days) followed by a 7-day (experiment I) and 14-day (experiment II) exponential phase and finally a stationary phase. The stationary
204 phase (early stationary phase) was reached after 14 and 21 days of growth in experiment I and II, respectively, and lasted until day 56 of cultivation in both experiments
205 (late stationary phase) (Figure 1A). Growth experiments I and II started with a similar cell density of approximately 10¹⁰ cells.L⁻¹ and demonstrated reproducible
206 growth patterns. At the time of inoculation, cell density was 9.51 × 10¹⁰ in experiment I and 7.11 × 10¹⁰ cells.L⁻¹ in experiment II (Figure 1A). *Synechococcus* grew
207 exponentially over the first 19 days in experiment I and over 21 days in experiment II until reaching a maximum of 1.9 × 10¹² and 1.5 × 10¹² cells.L⁻¹, respectively.
208 At the end of the exponential growth phase, the cell numbers levelled off and achieved a stable growth stage (stationary phase). Typical evolutions of pH values in
209 culture media during the *Synechococcus* growth experiments are presented in Figure 1B. As a general trend, pH is linked to the photosynthetic activity of cyanobacteria.
210 The pH levels rose rapidly during the exponential phase in both experiments, reaching around 10, and stayed steady during the stationary phase. While experiment I
211 experienced significant pH fluctuations during the latter part of the stationary phase, overall, the pH evolution trends for both experiments are comparable (Figure
212 1B).



213 **Figure 1.** Evolution of biomass of *Synechococcus* PCC 7942 culture in units of 10^{10} cells.L⁻¹ (A) and pH evolution (B) during exponential, early and late stationary phases. The vertical
 214 dotted lines (B) represent the stage transition between lag, exponential and stationary phases. Each value is the mean \pm SD of all replicate values.
 215

216 3.2 Extracellular carbonic anhydrase

217 The activity of extracellular carbonic anhydrase (eCA) in solution changed slightly over the growth experiment (Figure 1S). The highest eCA activity (~1600) was
 218 detected after 14 days of culture, during the exponential phase. The lowest activity was measured after 56 days of growth, in the late stationary phase.

219 3.3 Nutrient concentrations during growth

220 Nutrient concentration during the growth experiment is shown in Table 1. High nitrate concentrations supported exponential growth and high cell density. The results
 221 show that a major decrease in nitrate and phosphate concentrations occurred during the exponential growth phase and remained slowed down progressively over the
 222 stationary phase. At the end of the stationary phase, phosphate was virtually depleted, whereas 67% of nitrate was still available compared to its initial concentration.
 223 Ammonium concentration was below the limit of detection (0.05–40 μ g.L⁻¹). Ca²⁺ concentrations decreased gradually and accounted for the total calcium concentration
 224 of 81% in the late stationary phase.
 225

226 **Table 1.** Concentrations of NO₃⁻, PO₄³⁻ and Ca²⁺ (μ M) in the culture medium before inoculation (one-third-strength BG-11 medium) and at 0, 14, 28 and 56 days of *Synechococcus*
 227 growth experiment are given as mean concentrations of four replicates (n=4).

Major anions and cations (μ M)	Initial concentrations in the medium	<i>Synechococcus</i> growth phases		
		Exponential	Early stationary	Late stationary
NO ₃ ⁻	7082	5731	5544	4716
PO ₄ ³⁻	68	39	41	21
Ca ²⁺	102	91	88	83

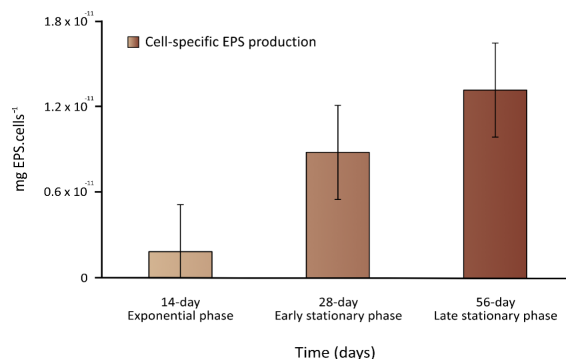
229 3.3 Abundance of EPS

230 The recovery yields of the EPS produced (mean \pm SD) resulting from the applied extraction method are listed in Table 2. The EPS yields varied from 2.9 \pm 0.5
 231 18.6 \pm 2.1 mg.L⁻¹ during exponential and early stationary phases and reached the highest yield of 35.4 \pm 4.2 mg.L⁻¹ at 56 days of culture, in the late stationary phase
 232 (Table 2). When the values were normalized per cell yield, data/results showed that the EPS concentration increased significantly between the exponential and late
 233 stationary phases (p-value < 0.05) (Figure 2). *Synechococcus* continuously produced EPS during the 56-day experiment. In the first 14 days of growth, cells grew
 234 exponentially and EPS production was deficient. Between exponential and early stationary phases, EPS production increased by a factor of five to seven, reaching a
 235 maximum in the late stationary phase, after the 56-day growth experiment.
 236

237 **Table 2.** Cell yield, total EPS production and cell-specific EPS production in *Synechococcus* PCC7942 cultures during exponential, early and late growth phases. Data represent the
 238 means of two independent experiments.

	Time of harvest (growth phase)		
	Exponential	Early stationary	Late stationary
Cell yield (cells.L ⁻¹)	(161.6 \pm 21.6)10 ¹⁰	(211.2 \pm 6.0)10 ¹⁰	(268.8 \pm 14.4)10 ¹⁰
EPS yield (mg.L ⁻¹)	2.9 \pm 0.5	18.6 \pm 2.1	35.4 \pm 4.2
Cell-specific EPS production (mg. cells ⁻¹)	(1.9 \pm 0.6)10 ⁻¹²	(8.8 \pm 0.8)10 ⁻¹²	(13.1 \pm 0.9)10 ⁻¹²

239
 240



241

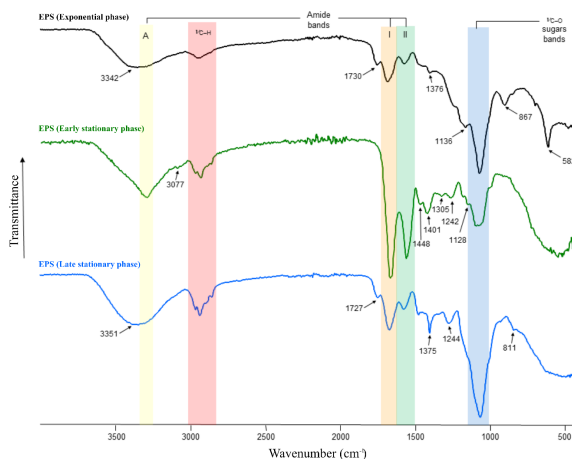
242

243 **Figure 2.** Cell-specific EPS production during the exponential, early and late stationary phases. MEAN±SD replicates from (n=2).

244 3.4 Chemical properties of EPS

245 3.4.1 FT-IR spectroscopy of EPS

246 FT-IR spectroscopy was used to check the overall EPS properties and composition. The IR spectra of EPS harvested during the exponential, early and late stationary
 247 phases of the growth experiment are depicted in Figure 3. The three spectra show strong similarities, exhibiting characteristic absorption bands for polysaccharides
 248 and protein moieties (highlighted in Figure 3 by vertical-coloured areas). However, differences in sample composition were also revealed by the presence of additional
 249 absorptions indicated by arrows in Figure 3. Interestingly, the spectrum of the exponential phase EPS exhibits a strong band, isolated at 582 cm⁻¹, which according to
 250 the literature on EPS could be assigned to a C–X stretch of alkyl halides (Kavita et al., 2011). Bands at 1039 – 1128 cm⁻¹ (C–O and C–O–C stretching vibrations)
 251 could be assigned to polysaccharides and polysaccharide-like structures (Wang et al., 2012b) and were observed in all EPS samples (Figure 3, blue area). In contrast,
 252 the small shoulders observed in the early and late stationary phase EPS, at ~1242 and 1244 cm⁻¹ correspond to sulfate groups. Bands at 811–868 cm⁻¹, most likely
 253 representing the glycosidic linkage between sugar monomers, were only present in EPS extracts in the early and late stationary phases. Low-intensity bands observed
 254 in the range of 1450–1370 cm⁻¹ are assigned to CH₃ and CH₂ deformations (bends) of proteins (Kansiz et al., 1999). These absorption bands were more evident in
 255 EPS obtained during the early stationary phase. The bands present in the range of 1660 and 1540 cm⁻¹ are attributed to C=O and C=N stretching vibrations and are
 256 characteristic of Amide I and II functions (Figure 3, orange and green areas, respectively), which are typically associated with proteins (Coates, 2000). Spectra of the
 257 early stationary phase EPS showed higher peaks of protein than those observed in EPS from exponential and late stationary phases. The medium bands at 1730 and
 258 1727 cm⁻¹, present in samples extracted from exponential and late stationary phases, can be attributed to C=O stretching vibrations resulting from lipids and fatty acids
 259 (Kansiz et al., 1999). Absorptions in the range of 2960–2850 cm⁻¹ corresponding to C–H stretching vibrations of aliphatic hydrocarbons and possibly indicative of
 260 long-chain polymers (e.g., sugars or proteins), were observable in all EPS extracts. The amide A band (3345 cm⁻¹), characteristic of the N–H vibration of peptide
 261 groups in proteins, is present in all spectra (Figure 3, yellow area), but is particularly visible on the early stationary phase EPS spectrum. In the samples at 14 and 56
 262 days of growth, this band is included in shoulders due to the presence of OH absorptions centred at 3342 and 3351 cm⁻¹, respectively. The list of band assignments is
 263 summarized in Table 1S (Supplementary data).



264

265 **Figure 3.** FT-IR spectra of EPS produced during the exponential (black line), early (green line) and late (blue line) stationary phases. Amide A absorbs in the range of 3342–3351
 266 cm⁻¹ (yellow area), amides I–II at 1542–1650 cm⁻¹ (orange and green areas), sulfate groups at ~1242–1244 cm⁻¹, polysaccharides at ~1040–1070 cm⁻¹ (blue area), and the β-glycosidic
 267 linkages are visible as a shoulder at ~867cm⁻¹.



268 **3.4.2 Protein, sugar and glycosaminoglycan (GAGs) contents**

269 Total protein and sugar contents in all EPS extracts were assessed by colorimetric assays. There were remarkable differences in the amounts of protein and these varied
 270 within the different growth phases (Table 3). The EPS produced during the exponential growth phase revealed the lowest concentration of protein ($79 \pm 9 \mu\text{g.mg EPS}^{-1}$).
 271 The highest protein concentration was measured in EPS produced during the early stationary phase ($253 \pm 42 \mu\text{g.mg EPS}^{-1}$), whereas during the late stationary phase
 272 EPS, the protein concentration decreased by ~ two-fold. When accounting for the cell yield at times of EPS extraction (Table 2), cells produced EPS with *ca* 11-15
 273 times more protein in the stationary phase than in the exponential phase (Table 3). The sugar content in the EPS harvested during the three different growth stages did
 274 not vary significantly (Table 3). The EPS produced during the exponential phase contained a slightly higher sugar content ($584 \pm 9 \mu\text{g}$ of xanthan and $504 \pm 78 \mu\text{g}$ of
 275 dextran equivalents. mg EPS^{-1}) than that measured in EPS produced during the early and late stationary phases (1.8 times and 1.3 times lower, respectively). These
 276 results demonstrate that sugars, rather than proteins, are the major component of all EPS extracts (Table 3). Our results show that, over the cultivation time, cells
 277 enhanced the production of larger amounts of glycosaminoglycans (GAGs) which can be associated with amino sugars and glycoproteins (Table 3). The highest
 278 fraction of sulfated groups (GAGs) to total EPS ($217 \pm 143 \mu\text{g GAGs.mg EPS}^{-1}$) was found in the late stationary phase EPS (Table 3). These results corroborate with
 279 data obtained from FTIR analysis.

280

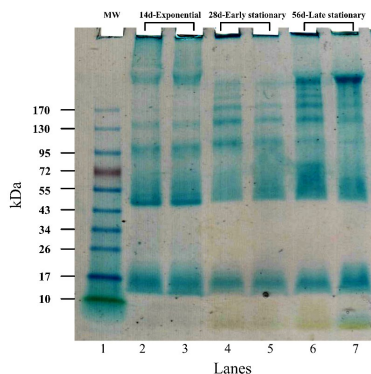
281 **Table 3.** Protein, sugar and glycosaminoglycan content of the harvested EPS at times 14, 28 and 56 days of *Synechococcus* PCC7942 culture. Values represent the average of two
 282 replicates (n=2).

Components of EPS yield	Time of EPS harvesting (days/growth phase)		
	14 days Exponential	28 days Early stationary	56 days Late stationary
Protein ($\mu\text{g.mg}^{-1}$ EPS)	79 ± 9	253 ± 42	128 ± 13
Cell-specific protein production ($\mu\text{g protein.cell}^{-1}$)	$(1.5 \pm 0.6) \times 10^{-10}$	$(2.2 \pm 0.1) \times 10^{-9}$	$(1.7 \pm 0.0) \times 10^{-9}$
Sugar ($\mu\text{g xanthan equivalents.mg}^{-1}$ EPS)	584 ± 95	326 ± 26	434 ± 11
Cell-specific sugar production ($\mu\text{g xanthan equivalent.cell}^{-1}$)	$(1.0 \pm 0.2) \times 10^{-9}$	$(2.8 \pm 0.1) \times 10^{-9}$	$(5.7 \pm 0.2) \times 10^{-9}$
Sugar ($\mu\text{g dextran equivalents.mg}^{-1}$ EPS)	504 ± 78	292 ± 22	381 ± 90
Cell-specific sugar production ($\mu\text{g dextran equivalent.cell}^{-1}$)	$(8.9 \pm 1.4) \times 10^{-10}$	$(2.6 \pm 0.1) \times 10^{-9}$	$(5.0 \pm 0.2) \times 10^{-9}$
Glycosaminoglycans ($\mu\text{g GAGs.mg}^{-1}$ EPS)	4 ± 0	31 ± 13	217 ± 143
Cell-specific GAGs production ($\mu\text{g GAGs.cell}^{-1}$)	$(5.5 \pm 5.5) \times 10^{-12}$	$(2.6 \pm 0.8) \times 10^{-10}$	$(3.0 \pm 2.0) \times 10^{-9}$
GAGs/Sugar (xanthan) ratio	0.01 ± 0.0	0.09 ± 0.0	0.51 ± 0.3
GAGs/Sugar (xanthan) ratio	0.01 ± 0.0	0.10 ± 0.0	0.58 ± 0.4

283

284 **3.4.3 SDS-PAGE**

285 The results of gel electrophoresis after the migration of exponential, early and late stationary phase EPS samples are illustrated in Figure 4. Replicates showed similar
 286 band patterns that are distributed between 10 and > 170 kDa. A sharp greenish band in the migration front is strongly stained in late stationary phase EPS (Figure 4,
 287 lanes 6 and 7) and may correspond to chlorophyll. A less pronounced smear is visible in extracts obtained from the early stationary phase (Figure 4, lanes 4 and 5).
 288 Bands of < 10 kDa were not detected in the EPS produced during the exponential phase (Figure 4, lanes 2 and 3). A marked smear pattern is evidenced in all EPS
 289 extracted between 10-26 kDa: one prominent band was individualized at 17 kDa. A discrete blue smear (> 17-43 or 55 kDa) is evidenced in exponential phase EPS
 290 samples (Figure 4, lanes 2 and 3) and is less obvious in EPS samples from the early and late stationary phase (lanes 4-5 and 6-7, respectively). No specific bands were
 291 individualized in this molecular mass range, for the three growth phases. A band at about 45-47 kDa was strongly stained in exponential phase only. It may represent
 292 an extracellular carbonic anhydrase (Kupriyanova et al., 2018) but this would need to be confirmed. Another possibility could be that the 45-47 kDa-band is chlorophyll
 293 f synthase, also referred to as ChfF, which seems to migrate around 46 kDa (Shen et al., 2019). An area between 43 and 170 kDa was noted in all EPS extracts,
 294 accounting for 5-6 individualized bands that may correspond to the consecutive addition of an identical 'module', because the progression is logarithmic: is clearly
 295 seen in the early and late stationary phase lanes (lanes 4-7). The individualized bands were densely stained in EPS from the late stationary phase, including a smear at
 296 ~43-55 or 72 kDa (Figure 4, lanes 6 and 7) and a prominent band at > 170 kDa (Figure 4, lanes 6 and 7).



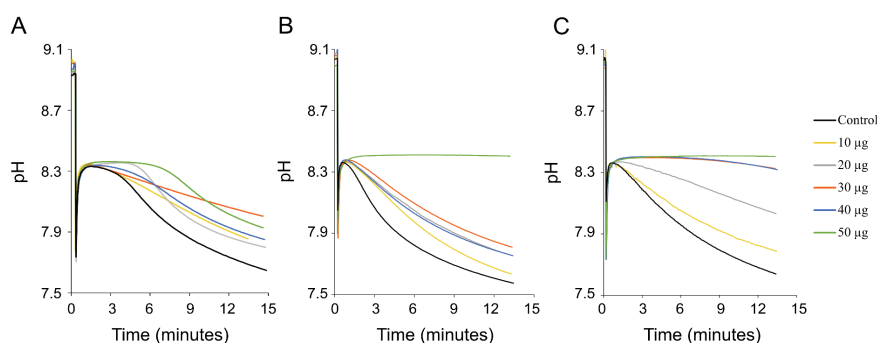
297

298 **Figure 4.** SDS-PAGE of EPS harvested during exponential (lanes 2-3), early (lanes 4-5) and late (lanes 6-7) stationary phases. Alcian blue staining was applied. The molecular ladder
 299 (MW) reference is shown in lane 1.



300 3.4.4 pH-drift assay

301 Recordings of the pH-drift assay are shown in Figure 5. The pH-drift assay determined the inhibitory effect of the EPS matrix (e.g., negatively charged functional
302 groups) on the rate of CaCO_3 precipitation. Negatively charged groups of EPS can bind calcium ions from the solution. The main phenomenon observed in this assay
303 is mineral-binding in which small calcium carbonate nuclei (nanometric or even pre-nucleation clusters) are very rapidly formed but they can be quickly poisoned by
304 EPS which do not allow them to grow more. We believe that in this case, their growth is simply stopped because soluble EPS molecules adsorb on mineral surfaces.
305 This mineral-binding also occurs due to the overall negative charge of the polymer of the matrix and is a much more efficient mechanism because of the ratio between
306 nanometric nuclei and EPS molecules in theory. In theory, one CaCO_3 mineral of few nanometres requires a great amount of Ca^{2+} ions for its formation. Thus, it is
307 more a “one-to-one” story (or something of that magnitude) between nanometric nuclei and single EPS molecules. Complete carbonate inhibition is reached when the
308 total Ca-binding capacity is achieved. CaCO_3 minerals start to nucleate, lowering the pH of the solution. Results show that the inhibitory effect was concentration-
309 dependent and clear differences were visible between EPS extracted in the exponential (Figure 5A), early (Figure 5B) and late (Figure 5C) growth phases. EPS matrices
310 from the stationary phase of culture growth (Figures 5B and 5C) exhibited a stronger inhibitory effect on CaCO_3 precipitation than the EPS extracted during the
311 exponential phase (Figure 5A). Complete inhibition was only reached in EPS from early and late stationary phases when $50 \mu\text{g}$ of $\text{EPS}\cdot\text{mL}^{-1}$ was tested. In this case,
312 a drop in pH was not observed and nucleation of crystals did not occur (Figure 5B and 5C), which means that the inhibition was total. Conversely, the exponential
313 phase EPS exhibited less inhibition of CaCO_3 precipitation (Figure 5A). The shorter plateau shows that the mineral-binding capacity of the matrix delayed CaCO_3
314 precipitation but that consequently the pH dropped and visible precipitates formed, showing a less powerful inhibitory effect of the EPS compared to stationary phases
315 EPS matrices.



316
317 **Figure 5.** *In vitro* inhibition of calcium carbonate precipitation by using EPS extracted during exponential (A), early (B) and late (C) stationary phases. Each panel shows the effect of
318 six different EPS concentrations (0, 10, 20, 30, 40 and $50 \mu\text{g}$) on CaCO_3 precipitation using the pH-drift assay method. The drop in pH indicates nucleation of CaCO_3
319 (= precipitation) and a plateau indicates inhibition of precipitation. A larger plateau indicates a higher Ca-binding capacity of the matrix and thus stronger inhibition. Complete
320 inhibition was observed when $50 \mu\text{g}$ of EPS solution from early and late stationary phases were used (e.g., see arrows). The results in each panel represent single experiments.
321 Replication showed identical results (see Supplementary Figure 2S).
322

323 3.5 Calcium carbonate crystallization in the presence of EPS

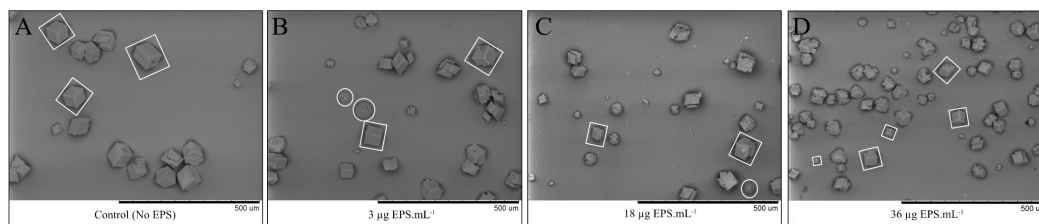
324 Forced CaCO_3 experiments were performed using a control solution (without EPS) and EPS solutions, at same pH, with concentrations of 3, 18 and $36 \mu\text{g}\cdot\text{mL}^{-1}$. Each
325 concentration corresponds to the EPS yield at different growth stages: exponential phase ($= 3 \mu\text{g}\cdot\text{EPS}\cdot\text{mL}^{-1}$), early ($18 \mu\text{g}\cdot\text{EPS}\cdot\text{mL}^{-1}$) and late ($36 \mu\text{g}\cdot\text{EPS}\cdot\text{mL}^{-1}$) stationary
326 phases. The crystals formed in the various EPS solutions showed different morphological (Figure 6) and mineralogical (Figure 3S) features as well as distinct crystal
327 sizes and distributions compared to those formed in control solution (Figure 7).

328 3.5.1 Mineral morphology

329 A preliminary light microscopic analysis was carried out in order to identify the most significant samples to analyse by SEM (Figure 6). The morphology of crystals
330 precipitated in the negative controls was very homogeneous and predominantly composed of calcite rhombohedrons that sometimes formed polycrystalline aggregates
331 of size $> 50 \mu\text{m}$ (Figure 6A). All control solutions tested for the various EPS harvested during exponential and stationary phases showed similar crystal characteristics.
332 In the EPS solutions, CaCO_3 crystals showed both rhombohedral and spheroidal morphologies (Figure 6B-D). The morphology of crystals appears to change with
333 increasing EPS concentrations. Spherical minerals formation was observed in the exponential phase-EPS solution (Figure 6B) and were less frequent in the EPS
334 solution from early stationary phase (Figure 6C). In the late stationary phase-EPS solution, rhombohedrons represented the prevalent crystal morphology while
335 spherical minerals were absent (Figure 6D).



336



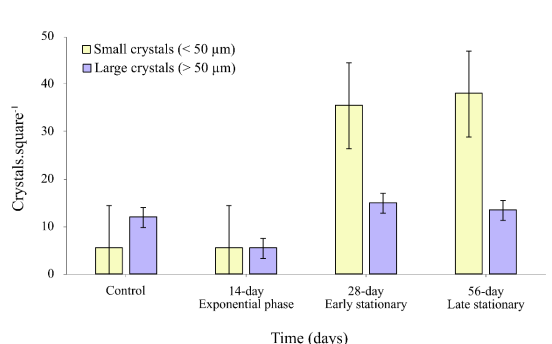
337
338 **Figure 6.** *In vitro* forced CaCO_3 precipitation assay in (A) the absence of the EPS (control solution) and in the presence of EPS extracted during the (B) exponential, (C) early and (D)
339 late stationary phases under increasing EPS concentrations of 3, 18 and 36 $\mu\text{g}\cdot\text{mL}^{-1}$, respectively. The images show two different CaCO_3 morphologies: rhombohedral (white squares)
340 and spheroidal (white circles), in some cases shown as polycrystalline crystals. The scale bar (black) at the bottom right of the images is 500 μm .

341 3.5.2 Crystal mineralogy

342 The crystals' mineralogy was assessed by FT-IR microscopy performed on selected individual crystals of $> 10 \mu\text{m}$ (Figure 3S). The results revealed that calcite was
343 the only CaCO_3 polymorph formed in the control solution. Calcite and vaterite formed in all EPS solutions tested. The FT-IR spectra revealed that all rhombohedrons
344 and polycrystalline aggregates with "sharp edges" represent calcite polymorphs. In contrast, spheroidal crystals revealed a vaterite signature (Figure 3S).

345 3.5.3 Crystal size and distribution

346 The results from image analysis showed that a larger quantity of crystals precipitated in the stationary phase (early and late) EPS solutions (Figure 7) and that major
347 differences were also observed in crystal size distribution (Figure 7). A comparison of the class of small crystal sizes ($< 50 \mu\text{m}$) with the large crystal size class
348 ($> 50 \mu\text{m}$) showed a clear trend of an increasing total number of small crystals in the stationary phase EPS solutions compared to those formed in the EPS solutions
349 from the exponential phase. The size reduction of the crystals at 18 and 36 mg/L (Figure 7, early and late stationary phases) suggests a partial inhibitory effect of the
350 EPS on the formation of calcium carbonate.



351
352 **Figure 7.** Total numbers of small ($< 50 \mu\text{m}$) and large ($> 50 \mu\text{m}$) crystal size classes of precipitated CaCO_3 in EPS solutions obtained from exponential and stationary phases, in EPS
353 concentrations of 3, 18 and 36 $\mu\text{g}\cdot\text{mL}^{-1}$, respectively.

354 4. Discussion

355 Our study demonstrates that the amount and properties of EPS change significantly ($p\text{-value} < 0.05$) at the three different stages of *Synechococcus* growth in an
356 artificial bloom experiment. Cells continuously produce EPS that increases in concentration and become more negatively charged in the stationary phase. We sampled
357 this EPS over the exponential, early and late stationary phases and studied its role in carbonate mineral precipitation. Based on this, a conceptual model was developed
358 to correlate the findings of this investigation with the potential EPS production of the naturally occurring picoplankton blooms and its possible involvement in whitening
359 events. Though natural blooms experience a variety of factors that are not represented in the experiments described in this paper, the first part of the discussion is
360 focussing only on the experimental data, whereas the interaction of these basic processes with other biotic and abiotic factors acting in the environment is discussed
361 afterwards.

362 4.1 Exponential growth phase

363 Macronutrients, such as nitrogen (N) and phosphorus (P) promote the initiation of cyanobacterial blooms (Reynolds and Walsby, 1975 ; Reynolds, 1987; Paerl, 1988;
364 Philips et al., 1999; Paerl, 2008; Xu et al., 2015). In our growth experiment, the beginning of the exponential phase (and the persistence of bloom) (Figure 1A) was
365 positively correlated with the high initial nutrient concentration in the medium (Table 1). Environmental factors such as water temperature, light intensity,
366 hydrodynamics and availability of dissolved inorganic carbon (DIC) are also important determinants of cyanobacteria bloom development (Clark and Flynn, 2000;



367 Dokulil and Teubner, 2000; Havens, 2008). Blooms can dramatically alter the supply of inorganic carbon for photosynthesis, which causes the pH to increase (Ibelings
368 and Maberly, 1998). In the early exponential phase of our batch cultures, the high photosynthetic activity of cyanobacteria cultures resulted in fast pH increase thereby
369 reducing the total inorganic carbon of the grown medium. Light and CO₂ are the sources of energy and carbon for cyanobacteria, and are of critical importance for
370 their growth (Takahashi et al., 2004). At pH 9 (Figure 1B), the concentration of CO₂ predicted is close to zero (< 1 μM) and the HCO₃⁻ concentration is 475 μM
371 (PhreeqC data). A similar scenario was observed in natural blooms occurrence: the population of cyanobacteria draws down the partial pressure of CO₂ (pCO₂) in the
372 photic zone, increasing the surface water pH up to 9-10 (Ibelings and Maberly, 1998; Verspagen et al., 2014) and CO₂ concentration can become completely depleted
373 or reach values close to zero (Maberly, 1996; Ibelings and Maberly, 1998; Verspagen et al., 2014). Under extreme conditions, the concentration of HCO₃⁻ can also
374 become markedly reduced (Talling, 1976; Maberly, 1996). When the rate of photosynthesis is greater than the combined rate of resupply of CO₂ from the atmosphere
375 and DIC in the hypolimnion, deviation from the air equilibrium occurs, favouring CaCO₃ precipitation. The pH of most aquatic systems ranges from 7.5-8.1 and keeps
376 inorganic carbon primarily in the form of bicarbonate (O'Neil et al., 2012). In poorly buffered systems, such as highly productive lakes, the pH and speciation of DIC
377 experience large fluctuations which vary widely on a scale from daily (diel) to episodic, to seasonal (Maberly, 1996) with diel variations as high as two pH units and
378 60 μmol DIC.L⁻¹ (Maberly, 1996). Because CO₂ favors the C₃ photosynthesis (C₃ cycle operation of Calvin-Beson cycle), the high pH of ~ 10 in our growth medium
379 could be associated with carbon limitation (Ibelings and Maberly, 1998b; Verspagen et al., 2014).

380
381 To alleviate CO₂ limitation, cyanobacteria have developed an efficient CO₂-concentrating mechanism (CCM) (Aizawa and Miyachi, 1986; Badger and Price, 1992;
382 Badger et al., 2002; Burnap et al., 2015) and can use bicarbonate as an inorganic carbon source for photosynthesis (Price et al., 1998, 2002; Giordano et al., 2005;
383 Sandrini et al., 2016). By activating CCM, cyanobacteria concentrate CO₂ by a factor of up to a thousand (Badger and Andrews, 1982; Badger et al., 2002, Price,
384 2011). CO₂-deficient conditions experienced during the exponential phase of our growth experiment, coupled with the continuous cellular demand for inorganic carbon
385 to support photosynthetic carbon fixation likely led the cells to activate CCM. The predicted concentrations of CO₂ and HCO₃⁻ in the growth medium (PhreeqC data)
386 in the early and late exponential phase infer that *Synechococcus* cells actively transported across the membrane and accumulated DIC into the cell, where the HCO₃⁻
387 pool was utilized to generate elevated CO₂ levels around Rubisco (Badger et al., 2002; Price et al., 2008). The CCM of cyanobacteria accomplishes very high carbon
388 concentrating factors (C_{external} : C_{internal}) at deficient specificity factors of RuBisCo (Tortell, 2000; Tortell et al., 2000). CCM involves bicarbonate transporters in the
389 cell membrane, intracellular (iCA) and extracellular (eCA) carbonic anhydrase enzymes and concentrated RuBisCO activity located in carboxisomes (Badger et al.,
390 2006; Price et al., 2008; Rae et al., 2013). CA converts HCO₃⁻ to CO₂ (Badger and Price, 1994), which increases the external pH in close proximity to the cells. In our
391 study, eCA activity was ~ 1.6-2.0 times higher during the exponential growth phase and reduced gradually through the stationary phase (Supplementary figure, Figure
392 S1). Similarly, Yang et al. (2023) measured the CA anhydrase in solution over a 30-day growth experiment with *Synechococcus* PCC 7942 and reported an increase
393 over the lag phase and large fluctuations over the exponential phase. During the stationary phase, CA did not vary greatly but a minor decrease was recorded in the
394 late stationary phase (Yang et al., 2023). In our study, the higher eCA activity recorded could explain the strongly stained ~45-47-kDa band that was only identified
395 in our SDS-PAGE gels of EPS produced during the exponential phase (Figure 4, lanes 2-3). The molecular weight (MW) of this band is similar to a 42-43 kDa eCA
396 previously identified by Kupriyanova et al. (2018) and discussed by Martinho de Brito et al. (2022). As explained in the Results section 3.4.3, we cannot exclude that
397 the band is chlorophyll *f* synthase, which seems to show up around 46 kDa. A more substantiated demonstration of the identity of the SDS-PAGE band will require
398 other approaches (beyond the scope of the present study), such as micro-sequencing of the purified 43 kDa band or the use of a CA-specific antibody.

399
400 Active uptake of HCO₃⁻ and accumulation of C_i species requires the input of metabolic energy e.g., ATP (BCT1 HCO₃⁻ transporter), NADPH or reduced ferredoxin
401 (CO₂ uptake) or coupling to an electrochemical Na⁺ gradient (SbtA or BicA HCO₃⁻ transport) (Badger et al., 2002; Price et al., 2008). This energetic cost may therefore
402 reflect on the growth rates achieved. *Synechococcus* PCC 7942 grows at > 80% of its maximum growth rate when provided with HCO₃⁻ as its main inorganic carbon
403 source (Miller et al., 1984). During the exponential phase, the carbon production from photosynthesis is mainly allocated for biomass production, not for EPS synthesis.
404 Our results showed the production of small amounts of EPS during the exponential phase (Figure 2, Table 2), which comprises a relatively larger amount of sugars
405 and lower protein and GAG contents than EPS from the stationary phase (Figure 3, Table 3). The smaller amount of negatively charged groups of the EPS during the
406 exponential phase (Figure 4, lanes 2-3) compared to those of EPS from the early and late stationary phases (Figure 4, lanes 4-7) resulted in weak to moderate inhibitory
407 capacity (Figure 5A). Consequently, our forced precipitation experiment with EPS from the exponential phase induced small amount of mostly large-sized carbonate
408 crystals (>50 μm), very similarly to the negative control experiment (Figure 7) (Martinho de Brito et al., 2022). The high concentration of Ca²⁺ in the medium (83
409 μM) compared to the initial [Ca²⁺] at the beginning of the experiment (103 μM), indicates that a small amount of calcium ions was bound to negatively charged
410 functional groups of EPS (Table 1, see [Ca²⁺]).

411 In our batch experiment, cells continue to grow exponentially for ~20 days of cultivation. At this point, cultures reached the maximum cell density (Figure 1A) and
412 pH values ranged between 10-11 (Figure 1B). Based on our calculations, under these alkaline conditions, CO₂ was completely depleted (1.7 × 10⁻³ μM) in the growth
413 medium, whereas HCO₃⁻ was extremely low (~ 79 μM). Thus, the dominant inorganic carbon speciation was CO₃²⁻ (421 μM). Because cells cannot take up CO₃²⁻ and
414 HCO₃⁻ concentration seems to be insufficient to cover the carbon demands of cyanobacterial growth, we assume that this may have been the cause of cell numbers
415 starting to level off (Figure 1A, early stationary phase). Consequently, cultures entered a stationary state due to a lack of inorganic carbon availability required to
416 increase cell population (Miller et al., 1984; Mayo et al., 1989; Verspagen et al., 2014). The excess of nutrients measured in the medium in the late exponential phase
417 (Table 1) suggested that the specific growth rate was not limited by nutrient availability but by a rather low level of CO₂ carbon content.

418
419

420 4.2 Early stationary phase

421 Insufficient CO₂ availability is considered to be the external stress factor constraining the growth rate of cyanobacteria (Maberly, 1996; Hein, 1997; Ibelings and
422 Maberly, 1998) and low [HCO₃⁻] could sustain a constant population density for at least ~ 40 days (See Figure 1A, stationary phase). Although cell numbers ceased
423 to increase (Figure 1A), the EPS production still increased; the total EPS yield was six times higher at the early stationary phase than in the exponential phase (Figure
424 2, Table 2). We assume that at this point, carbon fixation was allocated to EPS synthesis, not to biomass production (Miller et al., 1984). Increased EPS production is



425 usually associated with external stress factors (Rossi and De Philippis, 2015), including high pH conditions (Martinho de Brito et al., 2022). Moreover, metabolic
426 stress may also alter the composition of EPS (Babele et al., 2019; Martinho de Brito et al., 2022). In the present study, the negative functional group abundance
427 increased, resulting in a higher acidity of EPS (Figure 4, lanes 4-5) due to an increase in protein and sulfated glycan (GAG) (Table 3). In the pH conditions of the early
428 stationary phase, all the functional groups of the EPS matrix are deprotonated and are able to bind calcium ions (Figure 5B) (Dupraz and Visscher, 2005; Braissant et
429 al., 2003, 2007; Dittrich and Sibler, 2010) and bind calcium more efficiently nanometric nuclei in formation (if their formation is thermodynamically favoured). We
430 suggest that the increased calcium-binding capacity of the EPS probably accounts for lower the Ca^{2+} concentration measured in the medium (Table 2, see $[\text{Ca}^{2+}]$). In
431 our *in vitro* forced precipitation assay, we measure the second effect, the inhibitory one (mineral-binding effect), which results in the production of small-sized calcium
432 carbonate crystals ($< 50 \mu\text{m}$), in comparison to what happens in the exponential phase (Figure 7).

433 4.3 Late stationary phase

434 The late stationary phase of our experiment is characterized by minor fluctuations in cell density and pH values ($\text{pH} \sim 11$) (Figure 1A-B). The overall trend shows that
435 cells continued to produce more EPS, reaching a maximum concentration of one order of magnitude greater (twelve times higher) than in the exponential phase (Figure
436 2, Table 2). When raised to the cell-specific EPS production (in $\text{mg}\cdot\text{cells}^{-1}$), this ratio is about seven. As mentioned above, we assume that the continuous increase in
437 EPS production over the late stationary phase, including an overall augmentation of negatively charged functional groups (Figure 4, lanes 6-7), including GAG content
438 (Table 2), might be a specific response to a stress scenario. As expected, the present study shows that the greater amount of negatively charged functional groups of
439 EPS from the late stationary phase (Figure 4, lanes 6-7) resulted in a higher Ca-binding capacity than exponential and early stationary phase-EPS (Figure 5C). Our
440 forced precipitation experiments showed that minerals produced in the late stationary-EPS solutions are smaller and more abundant than those formed in EPS solutions
441 from the early stationary phase (Figure 7). Under natural conditions, when the Ca^{2+} supply is continuous, the crystals may or may not continue to grow, depending on
442 the physical space within the EPS matrix (Dupraz et al., 2009). Based on the high concentration of nitrate ($4720 \mu\text{M}$) measured in the late stationary phase (Table 1),
443 we assume that the abundance of this nutrient supported the persistence of the stationary phase, i.e., similar to a prolonged bloom in natural conditions. The death
444 phase was not observed in our 56-day-long experiment. Given that our cultures were continuously stirred, we can assume that light was not limiting cyanobacterial
445 growth. Furthermore, in natural blooms, the increase in population density may affect cells at greater depth through self-shading by decreasing the light available for
446 photosynthesis (Townsend et al., 1994). Yet, cyanobacteria (including *Synechococcus*) are known to be well-adapted to low-light conditions (Campbell and Carpenter,
447 1986; Palenik, 2001; Callieri et al., 2011). Additionally, the presence of sulfated constituents on late stationary phase-EPS contributes to a higher negative charge of
448 the matrix and higher Ca-binding potential (Decho and Kawaguchi, 2003; Braissant et al., 2007; Dupraz et al., 2009; Skoog et al., 2022), compared to EPS extracted
449 in the exponential phase which contained significantly lower GAG (Table 2). The present study shows that the greater amount of negatively charged functional groups
450 of EPS from the late stationary phase (Figure 4, lanes 6-7) resulted in a higher Ca-binding capacity than exponential and early stationary phase-EPS (Figure 5C). Our
451 forced precipitation experiments showed that minerals produced in the late stationary-EPS solutions are smaller and more abundant than those formed in EPS solutions
452 from the early stationary phase (Figure 7), suggesting an increased inhibitory ability of the late stationary-EPS.

453

454 4.4 Natural bloom and formation of whittings – Conceptual model

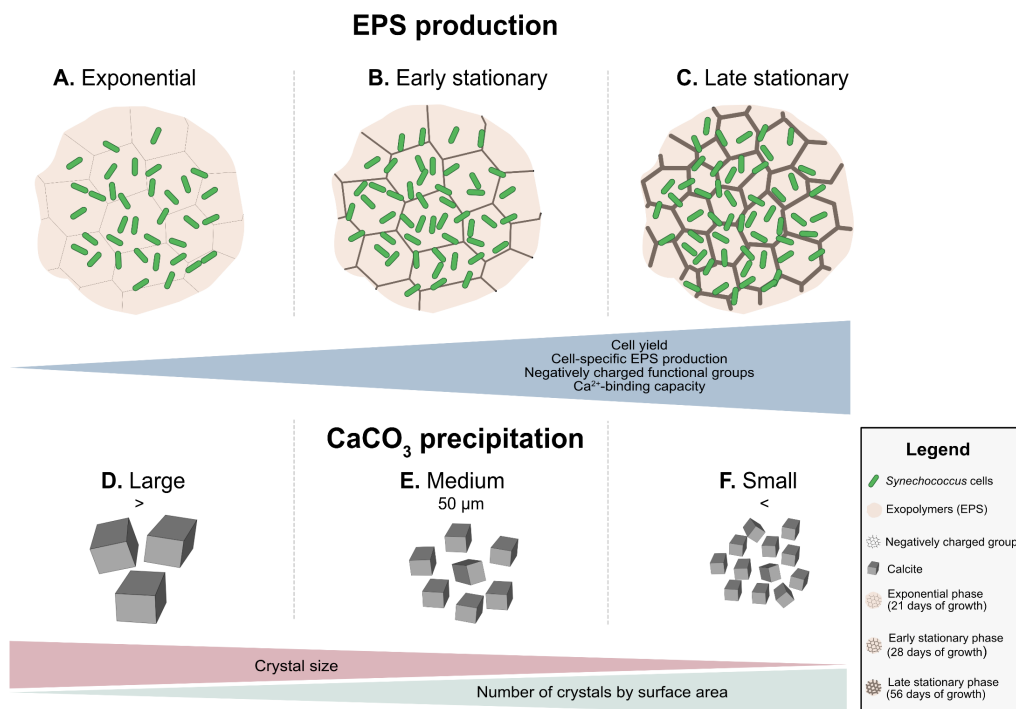
455 Our observations made during exponential and stationary phases can be applied to generate a conceptual model of EPS properties during a bloom event (Figure 8A-
456 C). The onset of a bloom starts with an increase in cell numbers, with high values in spring-summer (exceeding $10^5\cdot 10^7 \text{ cells}\cdot\text{mL}^{-1}$) and lower values in winter months
457 ($< 10^5 \text{ cells}\cdot\text{mL}^{-1}$) in both marine (Agawin et al., 1998; Philips et al., 1999) and freshwater (Maeda et al., 1992; Tai and Palenik, 2009) environments. This resembles
458 the exponential growth phase in our study (Figure 1, exponential phase). We predict that during the initial phase of a natural bloom, there is little EPS production:
459 cells grow relatively quickly and the carbon fixed during photosynthesis is predominantly allocated to biomass production (Figure 8A). The fast growth is followed
460 by a phase during which cell numbers level off, typically due to stress conditions, which is represented by the early stationary phase in our study. Under certain
461 conditions, blooms can be sustained for weeks and possibly longer (Anderson et al., 2002; Havens, 2008; Zhao et al., 2013), similar to what we observed in our growth
462 experiments (Figure 1A, early stationary phase). The maintenance of a bloom requires continuous input of nutrients, which is also the case in our experiment (Table
463 1) or in the case of natural systems, a turnover from lysing cells recycled by other microbes. During this phase, we did not observe a significant increase in cell density
464 but the production of EPS continued at a disproportionately high rate (Figure 8B-C). Our findings are in agreement with the lab studies using diatom cultures which
465 show that EPS production is low during exponential growth and increases in the stationary phase (Myklestad and Haug, 1972; Myklestad et al., 1989; Boshle et al.,
466 1995). These authors reported that nutrient-deficient conditions enhanced the production of EPS over the growth phases. If carbon fixation continues and some
467 critically required nutrient is lacking from the growth medium, most likely the phototrophic organisms produce carbohydrate reservoirs (Ciebiada et al., 2020). These
468 include storage polymers like glycogen and the production of other carbohydrate-rich compounds, including EPS (De Philippis et al., 1996, 1998, 2001; Decho and
469 Gutierrez, 2017). The decline of blooms in natural environments is typically associated with nutrient, low or high light intensity, grazing or viral infection. Under
470 these stressful conditions, an increase in EPS production by the phyto/picoplankton community may be expected.

471

472 Cyanobacterial blooms, including those of *Synechococcus* spp., can produce the so-called whiting events (Thompson and Ferris, 1990; Thompson et al., 1990; Robbins
473 and Blackwelder, 1992; Schultze-Lam et al., 1992; Thompson, 2000). A whiting is defined as the occurrence of a large number of CaCO_3 minerals in surface water
474 (Strong and Eadie, 1978). These often large-scale carbonate precipitation phenomena have been observed from space (Robbins et al., 1997; Dierssen et al., 2010). The
475 source and cause of whiting formation have been widely debated over the past decades and several biotic and physicochemical mechanisms have been proposed (Shinn
476 and Steinen, 1989; Larson and Mylroie, 2014). The most accepted mechanisms include chemical/spontaneous precipitation (Brunskill, 1969; Broecker et al., 2000),
477 physical disturbance and resuspension of carbonate sediments (Boss and Neumann, 1993; Broecker et al., 2000; Morse et al., 2003) and biologically-mediated CaCO_3
478 precipitation as a result of photosynthetic activity of picoplankton and phytoplankton community (Thompson and Ferris, 1990; Robbins and Blackwelder, 1992;
479 Schultze-Lam et al., 1992; Robbins et al., 1997; Thompson, 2000). However, the role of EPS in massive CaCO_3 production has been poorly investigated (Stanton et
480 al., 2021). Carefully transporting the results from forced precipitation experiments to a whiting event, we suggest that early in the bloom (Figure 8A), relatively large
481 CaCO_3 crystals form, provided sufficient Ca^{2+} is available (Figure 8D). As the bloom continues to grow, progressively the larger quantity of negatively charged



482 functional groups in the EPS provides more cation-binding sites and thus inhibits calcium carbonate precipitation to a greater extent. Depending on the three-
 483 dimensional structure of the EPS and surface properties (Wang et al., 2012), nucleation may yield smaller CaCO₃ crystals (Figure 8). If this occurs, then the production
 484 of a more negatively charged matrix (largely contributed by the enrichment in sulfated polysaccharides) may offer some selective advantage to the cyanobacteria
 485 population, by inhibiting and/or delaying mineral precipitation and by reducing crystal size formed around the cells. This might result in slow sinking rates, extending
 486 the residence time of the cyanobacterial community in the photic zone. If the bloom occurrence is short (e.g., similar to 14–28 days in our growth experiment), minerals
 487 making up the whiting will be relatively larger. Consequently, the aggregates of cyanobacteria, EPS and CaCO₃ minerals may sink faster because mineral precipitation
 488 in EPS increases the cyanobacterial-specific density several-fold. The *Synechococcus* specific density (ρ) is 1.040 g·cm⁻³ (Reynolds, 1987), near-neutrally buoyant,
 489 whereas ρ_{calcite} is 2.710 g·cm⁻³ (Lange, 1999). The production of larger amounts of more negatively charged EPS may act as a protection mechanism against carbonate
 490 formation in the vicinity of the cell wall (Martinez et al., 2010; Bundeleva et al., 2012), thus allowing the organisms to reside longer in the photic zone. Interestingly,
 491 the production of EPS that contained sulfated groups among bacteria seems to be exclusive to cyanobacteria (Pereira et al., 2009; Maeda et al., 2021). Maeda et al.
 492 (2021) reported that the cyanobacterium *Synechocystis* 6803 produced large amounts of GAG compounds during an experimental bloom formation. The authors
 493 suggested that these constituents can be advantageous for the development of surface bloom as it may increase the buoyancy, permitting cells to migrate upward
 494 rapidly when the water column is stable (Walsby et al., 1995). Thus, GAG production may be considered as an alternative for organisms that lack gas vesicles to
 495 remain longer in the photic zone (Maeda et al., 2021). The negative charge of EPS produced containing high sulfated content also protects the community against viral
 496 infection (Matsunaga et al., 1996). Therefore, the production of GAG by pelagic cyanobacteria contributes to stress tolerance and viral infectivity, helping in the
 497 persistence of bloom. In our growth experiments, a decline in cell numbers was not observed, which would represent the end of the bloom. In the natural environment,
 498 nutrient depletion, grazing or viral lysis/infection are the most likely causes of terminating a bloom (Gons et al., 2002). The cell lysis releases organic matter, which
 499 supports the growth of heterotrophic bacteria (Kjelleberg et al., 1987; Hagström et al., 1988; Kieft et al., 2021). Photosynthetically derived organic carbon is one of the
 500 major carbon and energy sources for heterotrophic bacteria (Allgaier et al., 2008). These heterotrophs can degrade EPS and liberate bound Ca²⁺ (Visscher et al. 1998;
 501 Arp et al., 2001; Dupraz et al., 2004; Braissant et al. 2009; Ionescu et al., 2015; Diaz et al., 2017). In addition, microbial respiration will produce HCO₃⁻/CO₂, increasing
 502 the saturation index of CaCO₃, and may enhance the whiting (Figure 8). Although our model is [somewhat] largely theoretical at this stage, its merit is to focus on an
 503 overlooked actor of whiting events, the EPS. Furthermore, it provides a conceptual framework to work with, for designing novel experiments and measurements both
 504 in natural systems and at the lab bench, to validate the molecular mechanisms involved in microbial bloom associated CaCO₃ formation in marine and lacustrine
 505 models.



506
 507 **Figure 8.** Conceptual diagram of proposed EPS-supported carbonate precipitation mechanism explaining the origin of whiting events.

508 **Data availability**

509 All raw data can be provided by the corresponding authors upon request.

510 **Author contributions**

511 M.M.d.B., I.B. and P.T.V. designed the study in a project directed by P.T.V., I.B. and E.V.; M.M.d.B., I.B., P.T.V., F.M., A.W. and L.P. developed the methodology;
 512 M.M.d.B. and I.B. carried out the laboratory measurements; M.M.d.B., P.T.V. and I.B. analysed the data; M.M.d.B. wrote the manuscript draft with significant



513 contributions of P.T.V. and I.B. M.M.d.B., P.T.V., I.B., E.V., F.M., A.W and L.P. reviewed and edited the manuscript. All authors have read and agreed to the
514 published version of the manuscript.

515 Competing interests

516 The authors declare that they have no conflict of interest.

517 Acknowledgements

518 We thank to Nelly Debrosse (Bourgogne Franche-Comté University, Dijon), Adrien Force (Bourgogne Franche-Comté University, Dijon) and Elodie Cognard
519 (Bourgogne Franche-Comté University, Dijon) for helping with the measurements; Michel Picquet and Christine Stern (ICMUB Institut de Chimie Moléculaire,
520 Bourgogne Franche-Comté University, Dijon, France) for their technical assistance with FT-IR analysis; Christophe Loup and Nadia Crini (Laboratoire Chrono-
521 environnement, UMR CNRS 6249, Bourgogne Franche-Comté University, Besançon, France) for their technical assistance with Ion chromatography and ICP analyses.

522 Financial support

523 This study is a contribution of the SEDS and SAMBA teams of Biogeosciences laboratory (Bourgogne Franche-Comté University, Dijon, France) to the I-SITE project
524 UB18016-BGSIS.

525 References

- 526 Addadi, L. and Weiner, S.: Interactions between acidic proteins and crystals: stereochemical requirements in biomineralization., *Proceedings of the National Academy of Sciences*,
527 82, 4110–4114, 1985.
- 528 Agawin, N., Duarte, C., and Agustí, S.: Growth and abundance of *Synechococcus* sp. in a Mediterranean Bay: seasonality and relationship with temperature, *Mar. Ecol. Prog. Ser.*,
529 170, 45–53, <https://doi.org/10.3354/meps170045>, 1998.
- 530 Aizawa, K. and Miyachi, S.: Carbonic anhydrase and CO₂ concentrating mechanisms in microalgae and cyanobacteria, *FEMS Microbiology Letters*, 39, 215–233,
531 <https://doi.org/10.1111/j.1574-6968.1986.tb01860.x>, 1986.
- 532 Albeck, S., Aizenberg, J., Addadi, L., and Weiner, S.: Interactions of various skeletal intracrystalline components with calcite crystals, *Journal of the American Chemical Society*, 115,
533 11691–11697, 1993.
- 534 Allen, M. M.: Simple Conditions for Growth of Unicellular Blue-Green Algae on Plates 1, 2, *Journal of phycology*, 4, 1–4, 1968.
- 535 Anderson, D. M., Glibert, P. M., and Burkholder, J. M.: Harmful algal blooms and eutrophication: Nutrient sources, composition, and consequences, *Estuaries*, 25, 704–726,
536 <https://doi.org/10.1007/BF02804901>, 2002.
- 537 Arp, G., Reimer, A., and Reitner, J.: Photosynthesis-induced biofilm calcification and calcium concentrations in Phanerozoic oceans, *Science*, 292, 1701–1704, 2001.
- 538 Babele, P. K., Kumar, J., and Chaturvedi, V.: Proteomic de-regulation in cyanobacteria in response to abiotic stresses, *Frontiers in Microbiology*, 1315, 2019.
- 539 Badger, M. R. and Andrews, T. J.: Photosynthesis and Inorganic Carbon Usage by the Marine Cyanobacterium, *Synechococcus* sp, *Plant Physiol.*, 70, 517–523,
540 <https://doi.org/10.1104/pp.70.2.517>, 1982.
- 541 Badger, M. R. and Price, G. D.: The CO₂ concentrating mechanism in cyanobacteria and microalgae, *Physiologia Plantarum*, 84, 606–615, 1992.
- 542 Badger, M. R. and Price, G. D.: The role of carbonic anhydrase in photosynthesis, *Annual review of plant biology*, 45, 369–392, 1994.
- 543 Badger, M. R., Hanson, D., and Price, G. D.: Evolution and diversity of CO₂ concentrating mechanisms in cyanobacteria, *Functional Plant Biology*, 29, 161–173, 2002.
- 544 Badger, M. R., Price, G. D., Long, B. M., and Woodger, F. J.: The environmental plasticity and ecological genomics of the cyanobacterial CO₂ concentrating mechanism, *Journal of*
545 *Experimental Botany*, 57, 249–265, <https://doi.org/10.1093/jxb/eri286>, 2006.
- 546 Bhosle, N. B., Sawant, S. S., Garg, A., and Wagh, A. B.: Isolation and Partial Chemical Analysis of Exopolysaccharides from the Marine Fouling Diatom *Navicula subinflata*, *Botanica*
547 *Marina*, 38, <https://doi.org/10.1515/botm.1995.38.1-6.103>, 1995.
- 548 Borman, A. H., Jong, E. W., Huizinga, M., Kok, D. J., Westbroek, P., and Bosch, L.: The Role in CaCO₃ Crystallization of an Acid Ca²⁺-Binding Polysaccharide Associated with
549 Cocoliths of *Emiliania huxleyi*, *Eur J Biochem*, 129, 179–183, <https://doi.org/10.1111/j.1432-1033.1982.tb07037.x>, 1982.
- 550 Boss, S. K. and Neumann, A. C.: Physical versus chemical processes of “whiting” formation in the Bahamas, *Carbonates Evaporites*, 8, 135–148, <https://doi.org/10.1007/BF03175171>,
551 1993.
- 552 Braissant, O., Cailleau, G., Dupraz, C., and Verrecchia, E. P.: Bacterially induced mineralization of calcium carbonate in terrestrial environments: the role of exopolysaccharides and
553 amino acids, *Journal of Sedimentary Research*, 73, 485–490, 2003.
- 554 Braissant, O., Decho, A. W., Dupraz, C., Glunk, C., Przekop, K. M., and Visscher, P. T.: Exopolymeric substances of sulfate-reducing bacteria: interactions with calcium at alkaline
555 pH and implication for formation of carbonate minerals, *Geobiology*, 5, 401–411, 2007.
- 556 Braissant, O., Decho, A. W., Przekop, K. M., Gallagher, K. L., Glunk, C., Dupraz, C., & Visscher, P. T.: Characteristics and turnover of exopolymeric substances in a hypersaline
557 microbial mat. *FEMS microbiology ecology*, 67(2), 293–307, 2009.
- 558 Broecker, W. S., Sanyal, A., and Takahashi, T.: The origin of Bahamian Whittings revisited, *Geophys. Res. Lett.*, 27, 3759–3760, <https://doi.org/10.1029/2000GL011872>, 2000.
- 559 Brunskill, G. J.: Fayetteville Green Lake, New York. II. Precipitation and sedimentation of calcite in a meromictic lake with laminated sediments 1: Sedimentation in Green Lake,
560 *Limnol. Oceanogr.*, 14, 830–847, <https://doi.org/10.4319/lo.1969.14.6.0830>, 1969.
- 561 Bundeleva, I. A., Shirokova, L. S., Bénézeth, P., Pokrovsky, O. S., Kompantseva, E. I., and Balor, S.: Calcium carbonate precipitation by anoxygenic phototrophic bacteria, *Chemical*
562 *Geology*, 291, 116–131, <https://doi.org/10.1016/j.chemgeo.2011.10.003>, 2012.
- 563 Bundeleva, I. A., Shirokova, L. S., Pokrovsky, O. S., Bénézeth, P., Ménez, B., Gérard, E., and Balor, S.: Experimental modeling of calcium carbonate precipitation by cyanobacterium
564 *Gloeocapsa* sp., *Chemical Geology*, 374–375, 44–60, <https://doi.org/10.1016/j.chemgeo.2014.03.007>, 2014.
- 565 Burnap, R., Hagemann, M., and Kaplan, A.: Regulation of CO₂ Concentrating Mechanism in Cyanobacteria, *Life*, 5, 348–371, <https://doi.org/10.3390/life5010348>, 2015.
- 566 Callieri, C. and Stockner, J.: Picocyanobacteria success in oligotrophic lakes: fact or fiction?, *J Limnol*, 59, 72, <https://doi.org/10.4081/jlimnol.2000.72.2000>.
- 567 Callieri, C., Lami, A., and Bertoni, R.: Microcolony Formation by Single-Cell *Synechococcus* Strains as a Fast Response to UV Radiation, *Appl Environ Microbiol*, 77, 7533–7540,
568 <https://doi.org/10.1128/AEM.05392-11>, 2011.



- 569 Campbell, L., & Carpenter, E. J.: Diel patterns of cell division in marine *Synechococcus* spp. (Cyanobacteria): use of the frequency of dividing cells technique to measure growth rate.
570 *Mar. Ecol. Prog. Ser.*, 32, 139–148, 1986.
- 571 Ciebada, M., Kubiak, K., and Daroch, M.: Modifying the Cyanobacterial Metabolism as a Key to Efficient Biopolymer Production in Photosynthetic Microorganisms, *IJMS*, 21, 7204,
572 <https://doi.org/10.3390/ijms21197204>, 2020.
- 573 Clark, D. R. and Flynn, K. J.: The relationship between the dissolved inorganic carbon concentration and growth rate in marine phytoplankton, *Proc. R. Soc. Lond. B*, 267, 953–959,
574 <https://doi.org/10.1098/rspb.2000.1096>, 2000.
- 575 Coates, J.: Interpretation of infrared spectra, a practical approach, 2000.
- 576 Coello-Camba, A. and Agustí, S.: Picoplankton Niche Partitioning in the Warmest Oligotrophic Sea, *Front. Mar. Sci.*, 8, 651877, <https://doi.org/10.3389/fmars.2021.651877>,
577 2021.
- 578 De Philippis, R., Sili, C., and Vincenzini, M.: Response of an exopolysaccharide-producing heterocystous cyanobacterium to changes in metabolic carbon flux, *Journal of Applied Phycology*, 8, 275–281, 1996.
- 580 De Philippis, R., Margheri, M. C., Materassi, R., and Vincenzini, M.: Potential of unicellular cyanobacteria from saline environments as exopolysaccharide producers, *Applied and Environmental Microbiology*, 64, 1130–1132, 1998.
- 582 De Philippis, R., Sili, C., Paperi, R., and Vincenzini, M.: Exopolysaccharide-producing cyanobacteria and their possible exploitation: a review, *Journal of Applied Phycology*, 13,
583 293–299, 2001.
- 584 Decho, A. W. and Gutierrez, T.: Microbial extracellular polymeric substances (EPS) in ocean systems, *Frontiers in microbiology*, 8, 922, 2017.
- 585 Decho, A. W. and Kawaguchi, T.: Extracellular polymers (EPS) and calcification within modern marine stromatolites, in: *Fossil and Recent Biofilms*, Springer, 227–240, 2003.
- 586 Diaz, M. R., Eberli, G. P., Blackwelder, P., Phillips, B., and Swart, P. K.: Microbially mediated organomineralization in the formation of ooids, *Geology*, 45, 771–774,
587 <https://doi.org/10.1130/G39159.1>, 2017.
- 588 Dierssen, H., Zimmerman, R., Drake, L., and Burdige, D.: Benthic ecology from space: optics and net primary production in seagrass and benthic algae across the Great Bahama Bank,
589 *Mar. Ecol. Prog. Ser.*, 411, 1–15, <https://doi.org/10.3354/meps08665>, 2010.
- 590 Dittrich, M. and Obst, M.: Are picoplankton responsible for calcite precipitation in lakes?, *AMBIO: A Journal of the Human Environment*, 33, 559–564, 2004.
- 591 Dittrich, M. and Sibling, S.: Calcium carbonate precipitation by cyanobacterial polysaccharides, *Geological Society, London, Special Publications*, 336, 51–63, 2010.
- 592 Dittrich, M., Müller, B., Mavrocordatos, D., and Wehrli, B.: Induced calcite precipitation by cyanobacterium *Synechococcus*, *Acta hydrochimica et hydrobiologica*, 31, 162–169, 2003.
- 593 Dokulil, M. T., & Teubner, K.: Cyanobacterial dominance in lakes. *Hydrobiologia*, 438, 1–12, 2000.
- 594 Dubois, M., Gilles, K. A., Hamilton, J. K., Rebers, P. t, and Smith, F.: Colorimetric method for determination of sugars and related substances, *Analytical chemistry*, 28, 350–356,
595 1956.
- 596 Dupraz, C. and Visscher, P. T.: Microbial lithification in marine stromatolites and hypersaline mats, *Trends in microbiology*, 13, 429–438, 2005.
- 597 Dupraz, C., Visscher, P. T., Baumgartner, L. K., and Reid, R. P.: Microbe-mineral interactions: early carbonate precipitation in a hypersaline lake (Eleuthera Island, Bahamas):
598 Microbe-mineral interactions, Eleuthera Island, Bahamas, *Sedimentology*, 51, 745–765, <https://doi.org/10.1111/j.1365-3091.2004.00649.x>, 2004.
- 599 Dupraz, C., Reid, R. P., Braissant, O., Decho, A. W., Norman, R. S., and Visscher, P. T.: Processes of carbonate precipitation in modern microbial mats, *Earth-Science Reviews*, 96,
600 141–162, <https://doi.org/10.1016/j.earscirev.2008.10.005>, 2009.
- 601 Giordano, M., Beardall, J., and Raven, J. A.: CO₂ concentrating mechanism in algae: Mechanisms, Environmental Modulation, and Evolution, *Annu. Rev. Plant Biol.*, 56, 99–131,
602 <https://doi.org/10.1146/annurev.arplant.56.032604.144052>, 2005.
- 603 Gons, H. J., Ebert, J., Hoogveld, H. L., van den Hove, L., Pel, R., Takkenberg, W., & Woldring, C. J.: Observations on cyanobacterial population collapse in eutrophic lake water.
604 *Antonie van Leeuwenhoek*, 81, 319–326, 2002.
- 605 Hagström, Å., Azam, F., Andersson, A., Wikner, J., and Rassoulzadegan, F.: Microbial loop in an oligotrophic pelagic marine ecosystem: possible roles of cyanobacteria and
606 nanoflagellates in the organic fluxes, *Mar. Ecol. Prog. Ser.*, 49, 171–178, <https://doi.org/10.3354/meps049171>, 1988.
- 607 Havens, K. E.: Cyanobacteria blooms: effects on aquatic ecosystems. Cyanobacterial harmful algal blooms: state of the science and research needs, 733–747, 2008.
- 608 Hein, M.: Inorganic carbon limitation of photosynthesis in lake phytoplankton, *Freshwater Biology*, 37, 545–552, <https://doi.org/10.1046/j.1365-2427.1997.00180.x>, 1997.
- 609 Heisler, J., Gilbert, P. M., Burkholder, J. M., Anderson, D. M., Cochlan, W., Dennison, W. C., Dortch, Q., Gobler, C. J., Heil, C. A., Humphries, E., Lewitus, A., Magnien, R., Marshall,
610 H. G., Sellner, K., Stockwell, D. A., Stoecker, D. K., and Suddleson, M.: Eutrophication and harmful algal blooms: A scientific consensus, *Harmful Algae*, 8, 3–13,
611 <https://doi.org/10.1016/j.hal.2008.08.006>, 2008.
- 612 Hodell, D. A., Schelske, C. L., Fahnenstiel, G. L., and Robbins, L. L.: Biologically induced calcite and its isotopic composition in Lake Ontario, *Limnology and Oceanography*, 43,
613 187–199, 1998.
- 614 Huisman, J., Codd, G. A., Paerl, H. W., Ibelings, B. W., Verspagen, J. M. H., and Visser, P. M.: Cyanobacterial blooms, *Nat Rev Microbiol*, 16, 471–483,
615 <https://doi.org/10.1038/s41579-018-0040-1>, 2018.
- 616 Ibelings, B. W. and Maberly, S. C.: Photoinhibition and the availability of inorganic carbon restrict photosynthesis by surface blooms of cyanobacteria, *Limnology and Oceanography*,
617 43, 408–419, 1998.
- 618 Ionescu, D., Spitzer, S., Reimer, A., Schneider, D., Daniel, R., Reitner, J., de Beer, D., and Arp, G.: Calcium dynamics in microbialite-forming exopolymer-rich mats on the atoll of
619 Kiribati, Republic of Kiribati, Central Pacific, *Geobiology*, 13, 170–180, <https://doi.org/10.1111/gbi.12120>, 2015.
- 620 Kamennaya, N., Ajo-Franklin, C., Northen, T., and Jansson, C.: Cyanobacteria as Biocatalysts for Carbonate Mineralization, *Minerals*, 2, 338–364,
621 <https://doi.org/10.3390/min2040338>, 2012.
- 622 Kansiz, M., Heraud, P., Wood, B., Burden, F., Beardall, J., and McNaughton, D.: Fourier Transform Infrared microspectroscopy and chemometrics as a tool for the discrimination of
623 cyanobacterial strains, *Phytochemistry*, 52, 407–417, [https://doi.org/10.1016/S0031-9422\(99\)00212-5](https://doi.org/10.1016/S0031-9422(99)00212-5), 1999.
- 624 Kavita, K., Mishra, A., and Jha, B.: Isolation and physico-chemical characterisation of extracellular polymeric substances produced by the marine bacterium *Vibrio parahaemolyticus*,
625 *Biofouling*, 27, 309–317, <https://doi.org/10.1080/08927014.2011.562605>, 2011.
- 626 Kawaguchi, T. and Decho, A. W.: Isolation and biochemical characterization of extracellular polymeric secretions (EPS) from modern soft marine stromatolites (Bahamas) and its
627 inhibitory effect on CaCO₃ precipitation, *Preparative Biochemistry and Biotechnology*, 32, 51–63, 2002.
- 628 Kieft, B., Li, Z., Bryson, S., Hettich, R. L., Pan, C., Mayali, X., and Mueller, R. S.: Phytoplankton exudates and lysates support distinct microbial consortia with specialized metabolic
629 and ecophysiological traits. *Proc. Natl. Acad. Sci. U.S.A.*, 118, e2101178118, <https://doi.org/10.1073/pnas.2101178118>, 2021.



- 630 Kupriyanova, E. V. and Pronina, N. A.: Carbonic anhydrase: Enzyme that has transformed the biosphere, *Russ J Plant Physiol*, 58, 197–209,
631 <https://doi.org/10.1134/S1021443711020099>, 2011.
- 632 Kupriyanova, E. V., Sinetova, M. A., Bedbenov, V. S., Pronina, N. A., and Los, D. A.: Putative extracellular α -Class carbonic anhydrase, EcaA, of *Synechococcus elongatus* PCC
633 7942 is an active enzyme: A sequel to an old story, *Microbiology*, 164, 576–586, 2018.
- 634 Lange, N. A.: Lange's handbook of chemistry, 15. ed., edited by: Dean, J. A., McGraw-Hill, New York, NY, 1999.
- 635 Larson, E. B. and Myroloe, J. E.: A review of whiting formation in the Bahamas and new models, *Carbonates Evaporites*, 29, 337–347, <https://doi.org/10.1007/s13146-014-0212-7>,
636 2014b.
- 637 Liu, L., Huang, Q., and Qin, B.: Characteristics and roles of *Microcystis* extracellular polymeric substances (EPS) in cyanobacterial blooms: a short review, *Journal of Freshwater
638 Ecology*, 33, 183–193, <https://doi.org/10.1080/02705060.2017.1391722>, 2018.
- 639 Lüring, M., Mello, M. M. e, van Oosterhout, F., de Senerpont Domis, L., and Marinho, M. M.: Response of Natural Cyanobacteria and Algae Assemblages to a Nutrient Pulse and
640 Elevated Temperature, *Front. Microbiol.*, 9, 1851, <https://doi.org/10.3389/fmicb.2018.01851>, 2018.
- 641 Maberly, S. C.: Diel, episodic and seasonal changes in pH and concentrations of inorganic carbon in a productive lake, *Freshwater Biology*, 35, 579–598, [https://doi.org/10.1111/j.1365-
2427.1996.tb01770.x](https://doi.org/10.1111/j.1365-
642 2427.1996.tb01770.x), 1996.
- 643 Maeda, H., Kawai, A., and Tilzer, M. M.: The water bloom of Cyanobacterial picoplankton in Lake Biwa, Japan, *Hydrobiologia*, 248, 93–103, <https://doi.org/10.1007/BF00006077>,
644 1992.
- 645 Marin, F., Corstjens, P., de Gaulejac, B., de Vrind-De Jong, E., and Westbrook, P.: Mucins and molluscan calcification: molecular characterization of mucoperlin, a novel mucin-like
646 protein from the nautilus shell layer of the fan mussel *Pinna nobilis* (Bivalvia, Pteriomorpha), *Journal of Biological Chemistry*, 275, 20667–20675, 2000.
- 647 Martínez, R. E., Gardés, E., Pokrovsky, O. S., Schott, J., and Oelkers, E. H.: Do photosynthetic bacteria have a protective mechanism against carbonate precipitation at their surfaces?,
648 *Geochimica et Cosmochimica Acta*, 74, 1329–1337, <https://doi.org/10.1016/j.gca.2009.11.025>, 2010.
- 649 Martinho de Brito, M., Bundeleva, I., Marin, F., Vennin, E., Wilmotte, A., Plasseraud, L., and Visscher, P. T.: Effect of Culture pH on Properties of Exopolymeric Substances from
650 *Synechococcus* PCC7942: Implications for Carbonate Precipitation, *Geosciences*, 12, 210, <https://doi.org/10.3390/geosciences12050210>, 2022.
- 651 Marvasi, M., Visscher, P. T., and Casillas Martínez, L.: Exopolymeric substances (EPS) from *Bacillus subtilis*: polymers and genes encoding their synthesis, *FEMS microbiology
652 letters*, 313, 1–9, 2010.
- 653 Mayo, W. P., Elrifi, I. R., and Turpin, D. H.: The Relationship between Ribulose Bisphosphate Concentration, Dissolved Inorganic Carbon (DIC) Transport and DIC-Limited
654 Photosynthesis in the Cyanobacterium *Synechococcus leopoliensis* Grown at Different Concentrations of Inorganic Carbon, *Plant Physiol.*, 90, 720–727,
655 <https://doi.org/10.1104/pp.90.2.720>, 1989.
- 656 Miller, A. G., Turpin, D. H., and Canvin, D. T.: Growth and Photosynthesis of the Cyanobacterium *Synechococcus leopoliensis* in HCO_3^- -Limited Chemostats, *Plant Physiol.*, 75,
657 1064–1070, <https://doi.org/10.1104/pp.75.4.1064>, 1984.
- 658 Mitterer, R. M. and Cunningham, R.: The interaction of natural organic matter with grain surfaces: implications for calcium carbonate precipitation, 1985.
- 659 Morse, J. W., Gledhill, D. K., and Millero, F. J.: CaCO_3 precipitation kinetics in waters from the great Bahama bank: *Geochimica et Cosmochimica Acta*, 67, 2819–2826,
660 [https://doi.org/10.1016/S0016-7037\(03\)00103-0](https://doi.org/10.1016/S0016-7037(03)00103-0), 2003.
- 661 Murphy, L. S. and Haugen, E. M.: The distribution and abundance of phototrophic ultraplankton in the North Atlantic1, 2: Phototrophic ultraplankton, *Limnol. Oceanogr.*, 30, 47–58,
662 <https://doi.org/10.4319/lo.1985.30.1.0047>, 1985.
- 663 Myklesstad, S., & Haug, A.: Production of carbohydrates by the marine diatom *Chaetoceros affinis* var. willei (Gran) Hustedt. I. Effect of the concentration of nutrients in the culture
664 medium. *Journal of Experimental Marine Biology and Ecology*, 9(2), 125–136, 1972.
- 665 Myklesstad, S., Holm-Hansen, O., Vårum, K. M., and Volcani, B. E.: Rate of release of extracellular amino acids and carbohydrates from the marine diatom *Chaetoceros affinis*, *J
666 Plankton Res*, 11, 763–773, <https://doi.org/10.1093/plankt/11.4.763>, 1989.
- 667 Obst, M., Dynes, J. J., Lawrence, J. R., Swerhone, G. D., Benzerara, K., Karunakaran, C., Kaznatcheev, K., Tyliczszak, T., and Hitchcock, A. P.: Precipitation of amorphous CaCO_3
668 (aragonite-like) by cyanobacteria: a STXM study of the influence of EPS on the nucleation process, *Geochimica et Cosmochimica Acta*, 73, 4180–4198, 2009.
- 669 O'Neil, J. M., Davis, T. W., Burford, M. A., and Gobler, C. J.: The rise of harmful cyanobacteria blooms: The potential roles of eutrophication and climate change, *Harmful Algae*,
670 14, 313–334, <https://doi.org/10.1016/j.hal.2011.10.027>, 2012.
- 671 Paerl, H.: Nutrient and other environmental controls of harmful cyanobacterial blooms along the freshwater–marine continuum. *Cyanobacterial harmful algal blooms: State of the
672 science and research needs*, 217–237, 2008.
- 673 Paerl, H. W.: Nuisance phytoplankton blooms in coastal, estuarine, and inland waters1: Nuisance blooms, *Limnol. Oceanogr.*, 33, 823–843,
674 <https://doi.org/10.4319/lo.1988.33.4part2.0823>, 1988.
- 675 Paerl, H. W. and Huisman, J.: Blooms Like It Hot, *Science*, 320, 57–58, <https://doi.org/10.1126/science.1155398>, 2008.
- 676 Paerl, H. W., Fulton, R. S., Moisaner, P. H., and Dyble, J.: Harmful Freshwater Algal Blooms, With an Emphasis on Cyanobacteria, *The Scientific World Journal*, 1, 76–113,
677 <https://doi.org/10.1100/tsw.2001.16>, 2001.
- 678 Palenik, B.: Chromatic Adaptation in Marine *Synechococcus* Strains, *Appl Environ Microbiol*, 67, 991–994, <https://doi.org/10.1128/AEM.67.2.991-994.2001>, 2001.
- 679 Pannard, A., Pédrone, J., Bormans, M., Briand, E., Claquin, P., and Lagadeuc, Y.: Production of exopolymers (EPS) by cyanobacteria: impact on the carbon-to-nutrient ratio of the
680 particulate organic matter, *Aquat Ecol*, 50, 29–44, <https://doi.org/10.1007/s10452-015-9550-3>, 2016.
- 681 Pereira, S., Zille, A., Micheletti, E., Moradas-Ferreira, P., De Philippis, R., and Tamagnini, P.: Complexity of cyanobacterial exopolysaccharides: composition, structures, inducing
682 factors and putative genes involved in their biosynthesis and assembly, *FEMS microbiology reviews*, 33, 917–941, 2009.
- 683 Philips, E. J., Badylak, S., and Lynch, T. C.: Blooms of the picoplanktonic cyanobacterium *Synechococcus* in Florida Bay, a subtropical inner-shelf lagoon, *Limnol. Oceanogr.*, 44,
684 1166–1175, <https://doi.org/10.4319/lo.1999.44.4.1166>, 1999.
- 685 Ploug, H.: Cyanobacterial surface blooms formed by *Aphanizomenon* sp. and *Nodularia spumigena* in the Baltic Sea: Small-scale fluxes, pH, and oxygen microenvironments, *Limnol.
686 Oceanogr.*, 53, 914–921, <https://doi.org/10.4319/lo.2008.53.3.0914>, 2008.
- 687 Pomar, L. and Hallock, P.: Carbonate factories: a conundrum in sedimentary geology, *Earth-Science Reviews*, 87, 134–169, 2008.
- 688 Price, G. D.: Inorganic carbon transporters of the cyanobacterial CO_2 concentrating mechanism, *Photosynth Res*, 109, 47–57, <https://doi.org/10.1007/s11220-010-9608-y>, 2011.
- 689 Price, G. D., Stiltmeier, D., Klughammer, B., Ludwig, M., and Badger, M. R.: The functioning of the CO_2 concentrating mechanism in several cyanobacterial strains: a review of
690 general physiological characteristics, genes, proteins, and recent advances, *Canadian Journal of Botany*, 76, 973–1002, 1998.
- 691 Price, G. D., Maeda, S., Omata, T., and Badger, M. R.: Modes of active inorganic carbon uptake in the cyanobacterium, *Synechococcus* sp. PCC7942, *Functional Plant Biol.*, 29, 131,
692 <https://doi.org/10.1071/PP01229>, 2002.



- 693 Price, G. D., Badger, M. R., Woodger, F. J., and Long, B. M.: Advances in understanding the cyanobacterial CO₂-concentrating-mechanism (CCM): functional components, Ci
694 transporters, diversity, genetic regulation and prospects for engineering into plants, *Journal of Experimental Botany*, 59, 1441–1461, <https://doi.org/10.1093/jxb/ern112>, 2008.
- 695 Rae, B. D., Long, B. M., Whitehead, L. F., Förster, B., Badger, M. R., and Price, G. D.: Cyanobacterial Carboxysomes: Microcompartments that Facilitate CO₂ Fixation, *Microb*
696 *Physiol.* 23, 300–307, <https://doi.org/10.1159/000351342>, 2013.
- 697 Raven, J. A., Beardall, J., and Sánchez-Baracaldo, P.: The possible evolution and future of CO₂-concentrating mechanisms, *Journal of Experimental Botany*, 68, 3701–3716, 2017.
- 698 Reynolds, C. S.: Cyanobacterial Water-Blooms, in: *Advances in Botanical Research*, vol. 13, Elsevier, 67–143, [https://doi.org/10.1016/S0065-2296\(08\)60341-9](https://doi.org/10.1016/S0065-2296(08)60341-9), 1987.
- 699 Reynolds, C. S. and Walsby, A. E.: Water-Blooms, *Biological Reviews*, 50, 437–481, <https://doi.org/10.1111/j.1469-185X.1975.tb01060.x>, 1975.
- 700 Rippka, R., Deruelles, J., Waterbury, J. B., Herdman, M., and Stanier, R. Y.: Generic assignments, strain histories and properties of pure cultures of cyanobacteria, *Microbiology*, 111,
701 1–61, 1979.
- 702 Robbins, L. and Blackwelder, P.: Biochemical and ultrastructural evidence for the origin of whittings: A biologically induced calcium carbonate precipitation mechanism, *Geology*,
703 20, 464–468, 1992.
- 704 Robbins, L. L., Tao, Y., and Evans, C. A.: Temporal and spatial distribution of whittings on Great Bahama Bank and a new lime mud budget, *Geol.* 25, 947, [https://doi.org/10.1130/0091-7613\(1997\)025<0947:TASDOW>2.3.CO;2](https://doi.org/10.1130/0091-7613(1997)025<0947:TASDOW>2.3.CO;2), 1997.
- 706 Rossi, F. and De Philippis, R.: Role of cyanobacterial exopolysaccharides in phototrophic biofilms and in complex microbial mats, *Life*, 5, 1218–1238, 2015.
- 707 Sandrini, G., Tann, R. P., Schuurmans, J. M., van Beusekom, S. A. M., Matthijs, H. C. P., and Huisman, J.: Diel Variation in Gene Expression of the CO₂-Concentrating Mechanism
708 during a Harmful Cyanobacterial Bloom, *Front. Microbiol.*, 7, <https://doi.org/10.3389/fmicb.2016.00551>, 2016.
- 709 Schultze-Lam, S., Harauz, G., and Beveridge, T. J.: Participation of a cyanobacterial S layer in fine-grain mineral formation, *J. Bacteriol.* 174, 7971–7981,
710 <https://doi.org/10.1128/jb.174.24.7971-7981.1992>, 1992.
- 711 Schultze-Lam, S., Schultze-Lam, S., Beveridge, T. J., and Des Marais, D. J.: Whiting events: biogenic origin due to the photosynthetic activity of cyanobacterial picoplankton,
712 *Limnology and oceanography*, 42, 133–141, 1997.
- 713 Shen, G., Canniffe, D. P., Ho, M.-Y., Kurashov, V., van der Est, A., Golbeck, J. H., and Bryant, D. A.: Characterization of chlorophyll f synthase heterologously produced in
714 *Synechococcus* sp. PCC 7002, *Photosynthesis research*, 140, 77–92, 2019.
- 715 Shinn, E. A., Steinen, R. P., Lidz, B. H., and Swart, P. K.: Whittings, a sedimentologic dilemma, *Journal of Sedimentary Research*, 59, 147–161, 1989.
- 716 Skoog, E. J., Moore, K. R., Gong, J., Ciccarese, D., Momper, L., Cutts, E. M., and Bosak, T.: Metagenomic, (bio)chemical, and microscopic analyses reveal the potential for the
717 cycling of sulfated EPS in Shark Bay pustular mats, *ISME COMMUN.*, 2, 43, <https://doi.org/10.1038/s43705-022-00128-1>, 2022.
- 718 Stal, L., Van Gemen, H., and Krumbein, W.: The simultaneous assay of chlorophyll and bacteriochlorophyll in natural microbial communities, *Journal of microbiological methods*,
719 2, 295–306, 1984.
- 720 Stanton, C., Barnes, B. D., Kump, L. R., and Cosmidis, J.: A re-examination of the mechanism of whiting events: A new role for diatoms in Fayetteville Green Lake (New York,
721 USA), *Geobiology*, 2021.
- 722 Strong, A. E. and Eadie, B. J.: Satellite observations of calcium carbonate precipitations in the Great Lakes 1: Satellite imagery, *Limnol. Oceanogr.*, 23, 877–887,
723 <https://doi.org/10.4319/lo.1978.23.5.0877>, 1978.
- 724 Tai, V. and Palenik, B.: Temporal variation of *Synechococcus* clades at a coastal Pacific Ocean monitoring site, *ISME J.* 3, 903–915, <https://doi.org/10.1038/ismej.2009.35>, 2009.
- 725 Takahashi, Y., Yamaguchi, O., and Omata, T.: Roles of CmpR, a LysR family transcriptional regulator, in acclimation of the cyanobacterium *Synechococcus* sp. strain PCC 7942 to
726 low-CO₂ and high-light conditions: High-light and low-CO₂ acclimation in cyanobacteria, *Molecular Microbiology*, 52, 837–845, <https://doi.org/10.1111/j.1365-2958.2004.04021.x>,
727 2004.
- 728 Talling, J. F.: The Depletion of Carbon Dioxide from Lake Water by Phytoplankton, *The Journal of Ecology*, 64, 79, <https://doi.org/10.2307/2258685>, 1976.
- 729 Thompson, J. and Ferris, F.: Cyanobacterial precipitation of gypsum, calcite, and magnesite from natural alkaline lake water, *Geology*, 18, 995–998, 1990.
- 730 Thompson, J. B.: Microbial whittings, *Microbial sediments*, 250–260, 2000.
- 731 Thompson, J. B., Ferris, F. G., and Smith, D. A.: Geomicrobiology and Sedimentology of the Mixolimnion and Chemocline in Fayetteville Green Lake, New York, *PALAIOS*, 5, 52,
732 <https://doi.org/10.2307/3514996>, 1990.
- 733 Tortell, P. D.: Evolutionary and ecological perspectives on carbon acquisition in phytoplankton, *Limnol. Oceanogr.*, 45, 744–750, <https://doi.org/10.4319/lo.2000.45.3.0744>, 2000.
- 734 Tortell, P. D., Rau, G. H., and Morel, F. M. M.: Inorganic carbon acquisition in coastal Pacific phytoplankton communities, *Limnol. Oceanogr.* 45, 1485–1500,
735 <https://doi.org/10.4319/lo.2000.45.7.1485>, 2000.
- 736 Townsend, D. W., Cammen, L. M., Holligan, P. M., Campbell, D. E., and Pettigrew, N. R.: Causes and consequences of variability in the timing of spring phytoplankton blooms,
737 *Deep Sea Research Part I: Oceanographic Research Papers*, 41, 747–765, [https://doi.org/10.1016/0967-0637\(94\)90075-2](https://doi.org/10.1016/0967-0637(94)90075-2), 1994.
- 738 Trichet, J. and Defarge, C.: Non-biologically supported organomineralization, *Bulletin-Institut Oceanographique Monaco-Numero Special*-, 203–236, 1995.
- 739 Verspagen, J. M. H., Van de Waal, D. B., Finke, J. F., Visser, P. M., Van Donk, E., and Huisman, J.: Rising CO₂ Levels Will Intensify Phytoplankton Blooms in Eutrophic and
740 Hypertrophic Lakes, *PLoS ONE*, 9, e104325, <https://doi.org/10.1371/journal.pone.0104325>, 2014.
- 741 Visscher, P. T., Reid, R. P., Bebout, B. M., Hoeff, S. E., Macintyre, I. G., & Thompson, J. A.: Formation of lithified micritic laminae in modern marine stromatolites (Bahamas); the
742 role of sulfur cycling. *American Mineralogist*, 83(11-12_Part_2), 1482-1493, 1998.
743
- 744 Walker, J. M., Marzec, B., Lee, R. B., Vodrazkova, K., Day, S. J., Tang, C. C., Rickaby, R. E., and Nudelman, F.: Polymorph selectivity of coccolith-associated polysaccharides from
745 *gephyrocapsa oceanica* on calcium carbonate formation in vitro, *Advanced Functional Materials*, 29, 1807168, 2019.
- 746 Wall, R. S. and Gyi, T. J.: Alcian blue staining of proteoglycans in polyacrylamide gels using the “critical electrolyte concentration” approach, *Analytical biochemistry*, 175, 298–299,
747 1988.
- 748 Wang, L.-L., Wang, L.-F., Ren, X.-M., Ye, X.-D., Li, W.-W., Yuan, S.-J., Sun, M., Sheng, G.-P., Yu, H.-Q., and Wang, X.-K.: pH dependence of structure and surface properties of
749 microbial EPS, *Environmental science & technology*, 46, 737–744, 2012a.
- 750 Wang, L.-P., Shen, Q.-R., Yu, G.-H., Ran, W., and Xu, Y.-C.: Fate of biopolymers during rapeseed meal and wheat bran composting as studied by two-dimensional correlation
751 spectroscopy in combination with multiple fluorescence labelling techniques, *Bioresource Technology*, 105, 88–94, <https://doi.org/10.1016/j.biortech.2011.11.064>, 2012b.
- 752 Weisse, T.: Dynamics of Autotrophic Picoplankton in Marine and Freshwater Ecosystems, in: *Advances in Microbial Ecology*, vol. 13, edited by: Jones, J. G., Springer US, Boston,
753 MA, 327–370, https://doi.org/10.1007/978-1-4615-2858-6_8, 1993.



- 754 Wells, A. J. and Iling, L. V.: Present-day precipitation of calcium carbonate in the Persian Gulf, 1964.
- 755 Wheeler, A., George, J. W., and Evans, C.: Control of calcium carbonate nucleation and crystal growth by soluble matrix of oyster shell, *Science*, 212, 1397–1398, 1981.
- 756 Whitton, B. A. and Potts, M.: Introduction to the Cyanobacteria, in: *Ecology of Cyanobacteria II*, edited by: Whitton, B. A., Springer Netherlands, Dordrecht, 1–13,
757 https://doi.org/10.1007/978-94-007-3855-3_1, 2012.
- 758 Xu, H., Paerl, H. W., Qin, B., Zhu, G., Hall, N. S., and Wu, Y.: Determining Critical Nutrient Thresholds Needed to Control Harmful Cyanobacterial Blooms in Eutrophic Lake Taihu,
759 China, *Environ. Sci. Technol.*, 49, 1051–1059, <https://doi.org/10.1021/es503744q>, 2015.
- 760 Yang, G., Li, F., Deng, Z., Wang, Y., Su, Z., Huang, L., Yin, L., and Ji, C.: Abnormal Crystallization Sequence of Calcium Carbonate in the Presence of *Synechococcus* sp. PCC 7942,
761 *Geomicrobiology Journal*, 40, 34–45, <https://doi.org/10.1080/01490451.2022.2100948>, 2023.
- 762 Yates, K. K. and Robbins, L. L.: Production of carbonate sediments by a unicellular green alga, *American Mineralogist*, 83, 1503–1509, 1998.
- 763 Zepernick, B. N., Gann, E. R., Martin, R. M., Pound, H. L., Krausfeldt, L. E., Chaffin, J. D., and Wilhelm, S. W.: Elevated pH Conditions Associated With *Microcystis* spp. Blooms
764 Decrease Viability of the Cultured Diatom *Fragilaria crotonensis* and Natural Diatoms in Lake Erie, *Frontiers in microbiology*, 12, 188, 2021.
- 765 Zhao, H., Han, G., Zhang, S., and Wang, D.: Two phytoplankton blooms near Luzon Strait generated by lingering Typhoon Parma: Lingering typhoon-induced algae blooms, *J.*
766 *Geophys. Res. Biogeosci.*, 118, 412–421, <https://doi.org/10.1002/jgrg.20041>, 2013.
- 767